Computers and Mathematics with Applications 172 (2024) 1–15

Contents lists available at ScienceDirect

Computers and Mathematics with Applications

journal homepage: www.elsevier.com/locate/camwa

Review and computational comparison of adaptive least-squares finite element schemes

Philipp Bringmann [1]

TU Wien, Institute of Analysis and Scientific Computing, Wiedner Hauptstr. 8–10, 1040, Vienna, Austria

ARTICLE INFO

Dataset link: https://doi.org/10.24433/CO.6310426.v1

Dedicated to Professor Leszek F. Demkowicz on the occasion of his 70th birthday

Keywords:
Least-squares finite element method
Adaptive mesh refinement
Alternative a posteriori error estimation
Separate marking
Data approximation
Numerical experiments

ABSTRACT

The convergence analysis for least-squares finite element methods led to various adaptive mesh-refinement strategies: Collective marking algorithms driven by the built-in a posteriori error estimator or an alternative explicit residual-based error estimator as well as a separate marking strategy based on the alternative error estimator and an optimal data approximation algorithm. This paper reviews and discusses available convergence results. In addition, all three strategies are investigated empirically for a set of benchmarks examples of second-order elliptic partial differential equations in two spatial dimensions. Particular interest is on the choice of the marking and refinement parameters and the approximation of the given data. The numerical experiments are reproducible using the author's software package octAFEM available on the platform Code Ocean.

1. Introduction

Least-squares finite element methods (LSFEMs) are highly popular discretisation schemes for partial differential equations. One key feature is their built-in a posteriori error estimation which renders this class of methods well-suited for adaptive mesh-refining algorithms. One of the first adaptive algorithms for LSFEMs has been proposed by Jiang and Carey [1]. The theoretical basis relies on the equivalence of the least-squares functional with the error in the standard Sobolev norm [2] resp. the equality with the error in the norm induced by the least-squares functional [3]. This property transfers to LSFEMs for regularised H^{-1} loads up to an oscillation term [4]. A particular scaling of the residuals enables the estimation of the contributions to the underlying norm separately [5]. Further algorithmic contributions deal with the iterative solution by algebraic multigrid [6] and parallelisation [7].

The built-in a posteriori error estimation and adaptive mesh refinement for standard LSFEMs have been established and investigated for a multitude of problems. The following non-exhaustive list illustrates the variety of applications. Adaptive LSFEMs in computational fluid mechanics deal with the shallow water equations [8,9], coupled Stokes-Darcy flow [10,11], viscoelastic fluids [12], interface problems [13], and fluid-structure interaction [14]. In computational solid mechanics, adaptive LSFEMs have been investigated for linear elasticity [15,16], elasto-plasticity [17], and the Signorini contact problem [18,19]. Further applications include convection-diffusion problems [20], parabolic problems [21–24], hyperbolic problems [25], the transport equation [26,27], the Poisson-Boltzmann equation [28], Maxwell and Helmholtz equation [29], convex energy minimisation [30], elliptic equations in nondivergence form [31], and the obstacle problem [32].

However, the advances in the convergence analysis with rates for adaptive FEMs in the past 15 years seem not to be applicable to this class of methods. This is because the built-in estimator lacks prefactors in terms of the mesh size inhibiting all known arguments for the proof of a local reduction of this estimator. In order to overcome this, an alternative explicit residual-based error estimator for an adaptive mesh-refining algorithm with optimal convergence rates is developed for the Poisson model problem in [33] and for further linear model problems in [34–36]. The known convergence results for h-adaptive LS-

The code (and data) in this article has been certified as Reproducible by Code Ocean: https://codeocean.com/. More information on the Reproducibility Badge Initiative is available at https://www.elsevier.com/physical-sciences-and-engineering/computer-science/journals.

E-mail address: philipp.bringmann@asc.tuwien.ac.at.

[1] **Acknowledgements.** It is my pleasure to acknowledge fruitful discussions with Prof. Carsten Carstensen and Dr. Rui Ma. This research has been supported by the Austrian Science Fund (FWF) through the project *Computational nonlinear PDEs* (grant P33216).

https://doi.org/10.1016/j.camwa.2024.07.022

Available online 5 August 2024

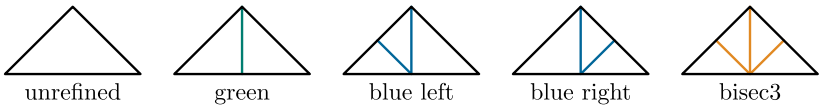

Fig. 1. Possible refinement of a triangle in 2D newest-vertex bisection.

FEMs are summarised and extended in the thesis [37] for the Poisson model problem, the Stokes equations, and the linear elasticity equations with discretisation of arbitrary polynomial degree and mixed boundary conditions in three spatial dimensions. All these algorithms employ a separate marking strategy with a quasi-optimal data approximation algorithm [38].

The negligence of the divergence contribution to the flux error allows for a collective marking strategy driven by the (slightly) modified alternative error estimator [39,40]. This guarantees optimal convergence rates in terms of the energy error plus the L^2 error of the flux variable.

The analysis of the alternative error estimator in [37] and in [39,40] requires the exact solution of the linear system of the FEM. However, a modified adaptive algorithm with collective marking in [41] allows for an iterative solver leading to optimal convergence rates with respect to the overall computational costs for a standard adaptive FEM.

While the plain convergence of adaptive LSFEM driven by the built-in estimator has recently been shown in [42,24] for any bulk parameter $0 < \theta \leq 1$, the only Q-linear convergence result in [43] requires a *sufficiently large* bulk parameter $0 \ll \theta \leq 1$. This contrasts the established convergence analysis in [44,38] asserting optimal rates for *sufficiently small* bulk parameters. The investigation of the bulk parameter is one goal of this paper.

Most but not all of the convergence results in Section 4 below hold for discretisations with arbitrary fixed polynomial degree. For the sake of concise statements, the presentation in this paper restricts to the lowest-order case.

Besides the theoretical review, this paper provides an experimental investigation of the performance of three adaptive LSFEM based on different error estimates applied to multiple benchmark problems. The influence of the chosen marking and refinement parameters is examined. A benchmark problem with a scalable microstructure in the right-hand side with exact integration allows the investigation of the data approximation employed in the adaptive algorithm with separate marking. Another focus is put on the performance of the implementation.

Beforehand, Section 2 introduces the notation for the triangulations and their adaptive refinement and Section 3 presents the least-squares discretisation of the Poisson model problem. The subsequent Section 4 presents the three investigated adaptive LSFEM algorithms and recalls the theoretical convergence results. The first subsection of Section 5 discusses some aspects of the implementation such as the employed numerical quadrature. The Subsections 5.2–5.5 present the results of the experiments. This paper ends with a conclusion in Section 6.

2. Triangulations and refinement

Given a bounded polygonal Lipschitz domain $\Omega \subset \mathbb{R}^2$, finite element discretisations typically base on shape-regular triangulations of Ω into closed triangles [45]. Let $\mathcal{T}_0$ be an initial triangulation of Ω. Note that the initial condition on $\mathcal{T}_0$ from [45, Sect. 4] is not required in 2D [46]. Given a set $\mathcal{M}_0 \subseteq \mathcal{T}_0$ of marked triangles, the refinement algorithm from [45, Sect. 6] creates the smallest regular refinement $\mathcal{T}_1$ of $\mathcal{T}_0$ such that all triangles in $\mathcal{M}_0 \subseteq \mathcal{T}_0 \setminus \mathcal{T}_1$ are refined. The algorithm employs the newest-vertex bisection (NVB) from [47–49]. This defines the concept of a one-level refinement [45, Sect. 2] leading to the set of admissible triangulations

$$\mathbb{T} := \{\mathcal{T}_\ell \text{ regular triangulation of } \Omega \text{ into closed triangles } :$$
$$\exists \ell \in \mathbb{N}_0 \exists \mathcal{T}_0, \mathcal{T}_1, \dots, \mathcal{T}_\ell \text{ successive one-level refinements}$$
$$\text{in the sense that } \mathcal{T}_{j+1} \text{ is a one-level refinement of } \mathcal{T}_j \text{ for}$$
$$j = 0, 1, \dots, \ell - 1\}.$$

It contains the finite subsets of triangulations with at most $N \in \mathbb{N}$ additional triangles

$$\mathbb{T}(N) := \{\mathcal{T} \in \mathbb{T} \,:\, |\mathcal{T}| - |\mathcal{T}_0| \leq N\}.$$

In 2D, the one-level refinements result in one of the five possible refinements as displayed in Fig. 1 for each triangle in $\mathcal{T}$. For a sequence of successively refined meshes $\mathcal{T}_\ell$ for $\ell \in \mathbb{N}_0$, the mesh-closure estimate bounds the number of newly created triangles [47,49]

$$|\mathcal{T}_\ell| - |\mathcal{T}_0| \leq C_{\mathrm{NVB}} \sum_{j=0}^{\ell-1} |\mathcal{M}_j|.$$

The process of marking triangles for bisection employs an error indicator $\eta(\mathcal{T}, T) \in \mathbb{R}$ for each $T \in \mathcal{T}$. For any subset $\mathcal{M} \subseteq \mathcal{T}$, abbreviate the corresponding contributions $\eta^2(\mathcal{T}, \mathcal{M}) := \sum_{T \in \mathcal{M}} \eta^2(\mathcal{T}, T)$ and $\eta^2(\mathcal{T}) := \eta^2(\mathcal{T}, \mathcal{T})$. Given a bulk parameter $0 < \theta \leq 1$, the Dörfler marking from [50] selects a subset $\mathcal{M} \subseteq \mathcal{T}$ with minimal cardinality [51] according to the criterion

$$\theta\, \eta^2(\mathcal{T}) \leq \eta^2(\mathcal{T}, \mathcal{M}). \tag{1}$$

For a triangulation $\mathcal{T} \in \mathbb{T}$, let $\mathcal{E}(T)$ denote the set of all edges of a triangle $T \in \mathcal{T}$. Let $\mathcal{E}$ denote the set of edges and $\mathcal{E}(\partial\Omega)$ the edges on the boundary $\partial\Omega$. Each triangle T has an outer unit normal vector ν_T and the orientation of each edge $E \in \mathcal{E}$ is fixed by one of the two possible orientations of the unit normal vector ν_E (and unit tangential τ_E). For an interior edge $E = \partial T_+ \cap \partial T_- \in \mathcal{E}(\Omega)$ shared by two triangles $T_+, T_- \in \mathcal{T}$ ensuring that $\nu_E = \nu_{T_+} = -\nu_{T_-}$. Accordingly $[w_h]_E := (w_h|_{T_+} - w_h|_{T_-})|_E$ defines the jump of any piecewise H^1 function w_h. Let $\omega_E := \mathrm{int}(T_+ \cup T_-)$ denote the patch of the interior edge E. Along the boundary $E \subset \partial\Omega$, the jump $[w_h]_E := w_h|_E$ is the trace of w_h on the unique triangle $T_+ \in \mathcal{T}$ with $E \in \mathcal{E}(T_+)$ and set $\omega_E := \mathrm{int}(T_+)$.

Throughout the paper, $A \lesssim B$ abbreviates the relation $A \leq C\, B$ with a positive generic constant $0 < C$ which solely depends on the initial triangulation $\mathcal{T}_0$, but is independent of the underlying piecewise constant mesh-size function $h_{\mathcal{T}} \in P_0(\mathcal{T})$ with $h_{\mathcal{T}}|_T := h_T := |T|^{1/2}$ for $T \in \mathcal{T} \in \mathbb{T}$. The context-sensitive measure $|\bullet|$ denotes not only the Lebesgue measure of Lebesgue sets in $\mathbb{R}^2$, but also the modulus of real numbers, the cardinality of finite sets, and the Euclidian norm of vectors in $\mathbb{R}^2$.

3. LSFEM for the Poisson model problem

For a right-hand side $f \in L^2(\Omega)$ on the polygonal Lipschitz domain $\Omega \subset \mathbb{R}^2$, the first-order system formulation of the Poisson model problem seeks $(p, u) \in H(\mathrm{div}, \Omega) \times H^1_0(\Omega)$ with

$$f + \mathrm{div}\, p = 0 \quad \text{and} \quad p - \nabla u = 0 \quad \text{in } \Omega. \tag{2}$$

This paper employs standard notation for Sobolev and Lebesgue spaces $H^1(\Omega)$, $H(\mathrm{div}, \Omega)$, and $L^2(\Omega)$. Appropriate subscripts designate their usual norms $\|\bullet\|_{H^1(\Omega)}$, $\|\bullet\|_{H(\mathrm{div},\Omega)}$, and $\|\bullet\|_{L^2(\Omega)}$.

Let $\mathcal{T} \in \mathbb{T}$ denote a regular triangulation of Ω into closed triangles. The lowest-order Raviart-Thomas function space $RT_0(\mathcal{T}) \subset H(\mathrm{div}, \Omega)$

and the conforming piecewise polynomials of first order $S^1_0(\mathcal{T}) \subset H^1_0(\Omega)$ allow for a unique discrete minimiser $(p_{\mathrm{LS}}, u_{\mathrm{LS}}) \in RT_0(\mathcal{T}) \times S^1_0(\mathcal{T})$ of the least-squares functional

$$LS(f; q_{\mathrm{LS}}, v_{\mathrm{LS}}) := \|f + \operatorname{div} q_{\mathrm{LS}}\|^2_{L^2(\Omega)} + \|q_{\mathrm{LS}} - \nabla v_{\mathrm{LS}}\|^2_{L^2(\Omega)}$$

over all $(q_{\mathrm{LS}}, v_{\mathrm{LS}}) \in RT_0(\mathcal{T}) \times S^1_0(\mathcal{T})$. The fundamental equivalence of the homogeneous least-squares functional [52, Lem. 4.3]

$$LS(0; q, v) \approx \|q\|^2_{H(\operatorname{div},\Omega)} + \|\nabla v\|^2_{L^2(\Omega)} \quad \text{for all } (q, v) \in H(\operatorname{div}, \Omega) \times H^1_0(\Omega) \tag{3}$$

provides well-posedness of the LSFEM. This ensures convergence towards the solution (p, u) of (2) in the case of (quasi-)uniform mesh refinement

$$\|p - p_{\mathrm{LS}}\|^2_{H(\operatorname{div},\Omega)} + \|\nabla(u - u_{\mathrm{LS}})\|^2_{L^2(\Omega)} \lesssim \inf_{\substack{q_{\mathrm{LS}} \in RT_0(\mathcal{T}) \\ v_{\mathrm{LS}} \in S^1_0(\mathcal{T})}} \big(\|p - q_{\mathrm{LS}}\|^2_{H(\operatorname{div},\Omega)} + \|\nabla(u - v_{\mathrm{LS}})\|^2_{L^2(\Omega)} \big).$$

Let $P_k(\mathcal{T})$ denote the space of piecewise polynomials with respect to the triangulation $\mathcal{T}$ and $\Pi : L^2(\Omega) \to P_0(\mathcal{T})$ the L^2-orthogonal projection onto $P_0(\mathcal{T})$. The piecewise constant approximation of some $f \in L^2(\Omega)$ leads to the data oscillations

$$\operatorname{osc}^2(f, \mathcal{T}) := \sum_{T \in \mathcal{T}} h_T^2 \, \|(1 - \Pi) f\|^2_{L^2(T)}. \tag{4}$$

4. Three adaptive algorithms

The following subsections introduce each of the adaptive LSFEMs, including the employed error estimators and the adaptive algorithm. They recall the theoretical convergence results.

4.1. Natural adaptive LSFEM

The contributions to the built-in a posteriori error estimator

$$\eta^2_{\mathrm{N}}(\mathcal{T}, T) := \|f + \operatorname{div} p_{\mathrm{LS}}\|^2_{L^2(T)} + \|p_{\mathrm{LS}} - \nabla u_{\mathrm{LS}}\|^2_{L^2(T)} \tag{5}$$

sum up to the least-squares functional

$$\eta^2_{\mathrm{N}}(\mathcal{T}) := \sum_{T \in \mathcal{T}} \eta^2_{\mathrm{N}}(\mathcal{T}, T) = LS(f; p_{\mathrm{LS}}, u_{\mathrm{LS}}).$$

The fundamental equivalence (3) ensures that this estimator is reliable and efficient even in the case of the inexact solution of the discrete problem

$$LS(f; q_{\mathrm{LS}}, v_{\mathrm{LS}}) \approx \|p - q_{\mathrm{LS}}\|^2_{H(\operatorname{div},\Omega)} + \|\nabla(u - v_{\mathrm{LS}})\|^2_{L^2(\Omega)}.$$

Moreover, the built-in error estimator is even asymptotically exact with respect to the norm on $H(\operatorname{div}, \Omega) \times H^1_0(\Omega)$ abbreviated by

$$|||(q, v)|||^2 := \|q\|^2_{H(\operatorname{div},\Omega)} + \|\nabla v\|^2_{L^2(\Omega)} \quad \text{for } (q, v) \in H(\operatorname{div}, \Omega) \times H^1_0(\Omega).$$

Theorem 4.1 *([29, Thm. 3.1]). For all $\varepsilon > 0$, there exists $\delta > 0$ such that every $\mathcal{T} \in \mathbb{T}$ with $\max_{T \in \mathcal{T}} \operatorname{diam}(T) \le \delta$ satisfies*

$$(1 - \varepsilon)|||(p - p_{\mathrm{LS}}, u - u_{\mathrm{LS}})|||^2 \le LS(f; p_{\mathrm{LS}}, u_{\mathrm{LS}}) \le (1 + \varepsilon)|||(p - p_{\mathrm{LS}}, u - u_{\mathrm{LS}})|||^2.$$

Theorem 4.1 applies to standard conforming discretisations of any order and various applications [29]. However, an earlier asymptotic exactness result in [53,54] relies on an unbalanced discretisation of the two variables p_{LS} and u_{LS}.

The collective marking for the natural estimator η_{N} from (5) results in the adaptive Algorithm 1 (NALSFEM). Independently of the choice of the bulk parameter θ, NALSFEM creates a convergent sequence of discrete solutions $(p_\ell, u_\ell)_\ell$ for $\ell \in \mathbb{N}_0$.

Algorithm 1 NALSFEM (natural adaptive LSFEM).

Input: regular triangulation $\mathcal{T}_0$ and bulk parameter $0 < \theta \le 1$.
for $\ell = 0, 1, 2, \dots$ **do**
Solve LSFEM with respect to triangulation $\mathcal{T}_\ell$ for solution (p_ℓ, u_ℓ).
Compute $\eta_{\mathrm{N}}(\mathcal{T}_\ell, T)$ from (5) for all $T \in \mathcal{T}_\ell$.
Mark minimal subset $\mathcal{M}_\ell \subseteq \mathcal{T}_\ell$ by the Dörfler criterion (1) for $\eta \equiv \eta_{\mathrm{N}}$.
Refine $\mathcal{T}_\ell$ to $\mathcal{T}_{\ell+1}$ by NVB such that $\mathcal{M}_\ell \subseteq \mathcal{T}_\ell \setminus \mathcal{T}_{\ell+1}$.
end for
Output: sequence of triangulations $\mathcal{T}_\ell$ with $(p_\ell, u_\ell)_\ell$ and $\eta_{\mathrm{N}}(\mathcal{T}_\ell)$ for $\ell \in \mathbb{N}_0$.

Theorem 4.2 *([42, Thm. 2], [24, Thm. 3.3]). For all $0 < \theta \le 1$, the output $(p_\ell, u_\ell)_\ell$ of NALSFEM satisfies*

$$\|p - p_\ell\|^2_{H(\operatorname{div},\Omega)} + \|\nabla(u - u_\ell)\|^2_{L^2(\Omega)} \to 0 \quad \text{as } \ell \to \infty.$$

The proofs in [42,24] employ the plain convergence framework from [55] under mild assumptions on the partial differential equation, the marking strategy, and the mesh refinement. It applies to higher-order discretisations as well as to more general marking criteria, e.g., the maximum marking strategy or the equilibrium marking strategy [42, Sect. 2.6].

If the NVB in the step **Refine** ensures the bisection of each edge of the marked triangles in $\mathcal{M}_\ell$, then NALSFEM converges Q-linearly in the following sense.

Theorem 4.3 *([43, Thm. 4.1]). Assume that the initial triangulation is sufficiently fine in that $f = \Pi_{L+1} f$ is resolved exactly on the level $\mathcal{T}_{L+1}$. There exist a minimal bulk parameter $0 < \Theta_0 < 1$, a reduction factor $0 < \varrho < 1$, and a constant $0 < \Lambda < \infty$ such that, for all $\Theta_0 \le \theta \le 1$, the modified estimator*

$$\widehat{\eta}^2_{\mathrm{N}}(\mathcal{T}_\ell) := LS(f; p_\ell, u_\ell) + \Lambda \, \|(1 - \Pi_\ell) p_\ell\|^2_{L^2(\Omega)}$$

with the output $(p_\ell, u_\ell)_\ell$ of NALSFEM satisfies

$$\widehat{\eta}^2_{\mathrm{N}}(\mathcal{T}_{\ell+1}) \le \varrho \, \widehat{\eta}^2_{\mathrm{N}}(\mathcal{T}_\ell) \quad \text{for all } \ell = L, L + 1, \dots$$

The key difficulty in the proof of convergence with rates as in Theorem 4.3 consists of the reduction of the natural estimator η_{N} on refined triangles. Within the frameworks [44,38], this relates to axiom (A2) for $0 < \varrho < 1$ and $0 < \Lambda$ such that

$$\eta_{\mathrm{N}}(\mathcal{T}_{\ell+1}, \mathcal{T}_{\ell+1} \setminus \mathcal{T}_\ell) \le \varrho \, \eta_{\mathrm{N}}(\mathcal{T}_\ell, \mathcal{T}_\ell \setminus \mathcal{T}_{\ell+1}) + \Lambda \, (LS(0; p_{\ell+1} - p_\ell, u_{\ell+1} - u_\ell))^{1/2}. \tag{6}$$

The lack of prefactors in terms of the mesh size prevent the usual arguments for the proof of (6) for η_{N}, cf. [56,57,44]. The earlier contributions [2] and [58] to the convergence analysis of adaptive LSFEMs prove the strict reduction, for $0 < \varrho < 1$,

$$\eta^2_{\mathrm{N}}(\mathcal{T}_{\ell+1}) \le \varrho \, \eta^2_{\mathrm{N}}(\mathcal{T}_\ell)$$

in each refinement step under the explicit assumption of a reduction property as (6) (called *local saturation* in [58]). Note that both works [2,58] employ a nonstandard marking routine and include severe restrictions on the refinement region (resp. on the shape of the domain Ω).

It turns out that the linear convergence (for small bulk parameter θ) already implies the optimal convergence rate.

Theorem 4.4 *([42, Prop. 15]). There exists a maximal bulk parameter $0 < \theta_0 < 1$ such that, for every $0 < \theta \le \theta_0$, the following implication holds. If the output $(p_\ell, u_\ell)_\ell$ of NALSFEM satisfies linear convergence with reduction factor $0 < \varrho < 1$, for all $\ell, m \in \mathbb{N}_0$,*

Algorithm 2 CALSFEM (collective marking adaptive LSFEM).

Input: regular triangulation $\mathcal{T}_0$ and bulk parameter $0 < \theta \le 1$.
for $\ell = 0, 1, 2, \dots$ **do**
Solve LSFEM with respect to triangulation $\mathcal{T}_\ell$ for solution (p_ℓ, u_ℓ).
Compute $\eta_C(\mathcal{T}_\ell, T)$ from (9) for all $T \in \mathcal{T}_\ell$.
Mark minimal subset $\mathcal{M}_\ell \subseteq \mathcal{T}_\ell$ by the Dörfler criterion (1) for $\eta \equiv \eta_C$.
Refine $\mathcal{T}_\ell$ to $\mathcal{T}_{\ell+1}$ by NVB such that $\mathcal{M}_\ell \subseteq \mathcal{T}_\ell \setminus \mathcal{T}_{\ell+1}$.
end for
Output: sequence of triangulations $\mathcal{T}_\ell$ with $(p_\ell, u_\ell)_\ell$ and $\eta_C(\mathcal{T}_\ell)$ for $\ell \in \mathbb{N}_0$.

$$\eta_N(\mathcal{T}_{\ell+m}) \lesssim \varrho^m \, \eta_N(\mathcal{T}_\ell), \tag{7}$$

then $(p_\ell, u_\ell)_\ell$ even converges with the optimal rate, i.e.,

$$\sup_{\ell \in \mathbb{N}_0} (1 + |\mathcal{T}_\ell| - |\mathcal{T}_0|)^s \eta_N(\mathcal{T}_\ell) \approx \sup_{N \in \mathbb{N}_0} (1+N)^s \min_{\mathcal{T} \in \mathbb{T}(N)} \eta_N(\mathcal{T}).$$

This result solely provides a *sufficient* condition for optimal convergence rates. However, the linear convergence (7) in the case of a small bulk parameter $0 < \theta < \theta_0 \ll 1$ remains an open question. In particular, the assumptions of a sufficiently large $0 \ll \Theta_0 \le \theta$ in Theorem 4.3 and of a sufficiently small $\theta \le \theta_0$ in Theorem 4.4 appear incompatible.

4.2. Alternative adaptive least-squares FEM with collective marking

In order to enable the reduction property of the form (6), the convergence analysis with rates for least-squares FEMs in [33,37,39,40] introduces alternative explicit a posteriori error estimators in terms of the constitutive residual

$$\begin{aligned}\eta_S^2(\mathcal{T}, T) := h_T^2 \, \| \operatorname{div}(p_{LS} - \nabla u_{LS}) \|_{L^2(T)}^2 + h_T^2 \, \| \operatorname{curl}(p_{LS} - \nabla u_{LS}) \|_{L^2(T)}^2 \\ + h_T \sum_{E \in \mathcal{E}(T) \setminus \mathcal{E}(\partial\Omega)} \| [p_{LS} - \nabla u_{LS}]_E \cdot \nu_E \|_{L^2(E)}^2 \\ + h_T \sum_{E \in \mathcal{E}(T)} \| [p_{LS} - \nabla u_{LS}]_E \cdot \tau_E \|_{L^2(E)}^2\end{aligned} \tag{8}$$

The second term $\| \operatorname{curl}(p_{LS} - \nabla u_{LS}) \|_{L^2(T)}^2$ vanishes in the lowest-order case with $(p_{LS}, u_{LS}) \in RT_0(\mathcal{T}) \times S_0^1(\mathcal{T})$. The discretisation of eigenvalue problems in [59], based on first-order system least-squares formulations, loses the built-in error estimation property (3). As a remedy, an alternative error estimator similar to η_S enables a posteriori error estimates in [59, Sect. 5].

If the error in the flux variable is solely measured in the L^2 norm (and not the full $H(\operatorname{div})$ norm) the data oscillation term (4) has to be included in the alternative error estimator [39,40]

$$\begin{aligned}&\eta_C^2(\mathcal{T}) := \sum_{T \in \mathcal{T}} \eta_C^2(\mathcal{T}, T) \quad \text{with} \\ &\eta_C^2(\mathcal{T}, T) := \eta_S^2(\mathcal{T}, T) + h_T^2 \| (1 - \Pi) f \|_{L^2(T)}^2.\end{aligned} \tag{9}$$

This provides a reliable and efficient error estimator in the corresponding reduced norm [39, Eqn. (5)]

$$\begin{aligned}LS(\Pi f; p_{LS}, u_{LS}) &\lesssim \| p - p_{LS} \|_{L^2(\Omega)}^2 + \| \nabla(u - u_{LS}) \|_{L^2(\Omega)}^2 \lesssim \eta_C^2(\mathcal{T}) \\ &\lesssim LS(\Pi f; p_{LS}, u_{LS}) + \operatorname{osc}^2(f, \mathcal{T}).\end{aligned}$$

Replacing the built-in error estimator η_N in Algorithm 1 by η_C leads to an alternative adaptive Algorithm 2 with collective marking (CALSFEM). The estimator η_C guarantees optimal convergence rates of CALSFEM with respect to the reduced norm.

Theorem 4.5 *([39, Sect. 2.5]). For all $0 < \theta \le 1$, there exists $0 < \varrho < 1$ such that the output $(p_\ell, u_\ell)_\ell$ of CALSFEM converges R-linearly, for all $\ell, m \in \mathbb{N}_0$,*

Algorithm 3 SALSFEM (separate marking adaptive LSFEM).

Input: regular triangulation $\mathcal{T}_0$, bulk parameter $0 < \theta \le 1$, reduction parameter $0 < \rho < 1$, and separation parameter $0 < \kappa$.
for $\ell = 0, 1, 2, \dots$ **do**
Solve LSFEM with respect to triangulation $\mathcal{T}_\ell$ for solution (p_ℓ, u_ℓ).
Compute $\eta_S(\mathcal{T}_\ell, T)$ from (8) for all $T \in \mathcal{T}_\ell$.
if Case A $\mu^2(\mathcal{T}) \le \kappa \, \eta_S^2(\mathcal{T})$ **then**
Mark minimal subset $\mathcal{M}_\ell \subseteq \mathcal{T}_\ell$ by Dörfler criterion (1) for $\eta \equiv \eta_S$.
Refine $\mathcal{T}_\ell$ to $\mathcal{T}_{\ell+1}$ by NVB such that $\mathcal{M}_\ell \subseteq \mathcal{T}_\ell \setminus \mathcal{T}_{\ell+1}$.
else (Case B $\kappa \, \eta_S^2(\mathcal{T}) < \mu^2(\mathcal{T})$)
Compute a refinement $\mathcal{T}_{\ell+1}$ of $\mathcal{T}_\ell$ of (almost) minimal cardinality with $\mu(\mathcal{T}_{\ell+1}) \le \rho \, \mu(\mathcal{T}_\ell)$.
end if
end for
Output: sequence of triangulations $\mathcal{T}_\ell$ with $(p_\ell, u_\ell)_\ell$, $\eta_S(\mathcal{T}_\ell)$, and $\mu(\mathcal{T}_\ell)$ for $\ell \in \mathbb{N}_0$.

$$\eta_C(\mathcal{T}_{\ell+m}) \lesssim \rho^m \, \eta_C(\mathcal{T}_\ell).$$

Moreover, there exists a maximal bulk parameter $0 < \theta_0 < 1$ such that, for every $0 < \theta \le \theta_0$, the sequence $(p_\ell, u_\ell)_\ell$ converges with the optimal rate, i.e., for every $0 < s < 1$,

$$\sup_{\ell \in \mathbb{N}_0} (1 + |\mathcal{T}_\ell| - |\mathcal{T}_0|)^s \eta_C(\mathcal{T}_\ell) \approx \sup_{N \in \mathbb{N}_0} (1+N)^s \min_{\mathcal{T} \in \mathbb{T}(N)} \eta_C(\mathcal{T}).$$

Theorem 4.5 generalises to higher-order discretisations in three spatial dimensions [40, Sect. 2.8].

4.3. Alternative adaptive least-squares FEM with separate marking

The optimal convergence rate of an adaptive algorithm in the full $H(\operatorname{div})$ norm for the flux variable requires the reduction of the data approximation error

$$\mu^2(\mathcal{T}) := \sum_{T \in \mathcal{T}} \mu^2(T) \quad \text{with} \quad \mu^2(T) := \| (1 - \Pi) f \|_{L^2(\Omega)}^2. \tag{10}$$

The sum of this data error with the residual error estimator from (8) provides a reliable and efficient error estimator [33, Thm. 3.1]

$$\mu^2(\mathcal{T}) + \eta_S^2(\mathcal{T}) \approx LS(f; p_{LS}, u_{LS}).$$

Since the data error term $\mu^2(T)$ lacks any prefactor in terms of the mesh size, its strict reduction in the sense of the axioms of adaptivity remains unclear. In order to achieve optimal convergence rates, Algorithm 3 (SALSFEM) employs a separate marking strategy [60,38]. If the residual error estimator $\eta_S^2(\mathcal{T})$ dominates the data error $\mu^2(\mathcal{T})$, the former is refined by the standard Dörfler marking and NVB. Otherwise, the latter is reduced by a suitable data approximation algorithm. The data approximation in Case B of SALSFEM employs the approximation algorithm (AA) from [61]. It consists of a slight modification of the Thresholding Second Algorithm (TSA) from [62] and utilises binary bins to guarantee linear computational complexity [62, Rem. 5.3]. The algorithm considers the refinement indicator $\widetilde{\mu}(T_j)$ for the two children T_1 and T_2 of a bisected parent triangle T defined, for $j = 1, 2$, by

$$\widetilde{\mu}(T_j) := (\mu(T_1) + \mu(T_2)) \, \widetilde{\mu}(T) / (\mu(T) + \widetilde{\mu}(T)) \tag{11}$$

with $\widetilde{\mu}(T) := \mu(T)$ for all initial triangles $T \in \mathcal{T}_0$. The TSA is followed by a completion step in order to ensure the output triangulation to be shape-regular. The resulting Algorithm 4 (AA) is instance optimal [62, 63]. Then Algorithm 3 SALSFEM converges with the optimal rate.

Theorem 4.6 *([33, Thm. 6.1]). For all $0 < \theta \le 1$, $0 < \kappa$, and $0 < \rho < 1$, there exists $0 < \varrho < 1$ such that the output $(p_\ell, u_\ell)_\ell$ of SALSFEM converges R-linearly, for all $\ell, m \in \mathbb{N}_0$,*

$$\mu^2(\mathcal{T}_{\ell+m}) + \eta_S^2(\mathcal{T}_{\ell+m}) \lesssim \varrho^m \left(\mu^2(\mathcal{T}_\ell) + \eta_S^2(\mathcal{T}_\ell) \right).$$

Algorithm 4 Approximation Algorithm (AA).

Input: initial regular triangulation $\mathcal{T}_0$, error tolerance Tol > 0
  Compute $\mu(T) = \widetilde{\mu}(T)$ for all $T \in \mathcal{T}_0$ and set $\widehat{\mathcal{T}} := \mathcal{T}_0$.
  while $\mu(\widehat{\mathcal{T}}) >$ Tol **do**
    Select the minimal $k \in \mathbb{Z}$ such that $\widetilde{\mu}(T) < 2^{k+1}$ for all $T \in \widehat{\mathcal{T}}$.
    Mark the set $\mathcal{M} := \{T \in \widehat{\mathcal{T}} \,:\, 2^k \le \widetilde{\mu}(T) < 2^{k+1}\}$.
    Bisect all triangles in $\mathcal{M}$ to obtain a new $\widehat{\mathcal{T}}$.
    Compute $\mu(T)$ and $\widetilde{\mu}(T)$ from (11) for all newly created $T \in \widehat{\mathcal{T}}$
  end while
  Apply **completion** on $\widehat{\mathcal{T}}$ to obtain a regular refinement $\mathcal{T}_{\mathrm{Tol}}$ of $\mathcal{T}_0$.
Output: $\mathcal{T}_{\mathrm{Tol}}$

Moreover, there exists a maximal bulk parameter $0 < \theta_0 < 1$ *and a maximal separation parameter* $0 < \kappa_0$ *such that for all* $0 < \theta \le \theta_0$, $0 < \kappa \le \kappa_0$, *and* $0 < \rho < 1$, *the sequence* $(p_\ell, u_\ell)_\ell$ *converges with the optimal rate, i.e., for all* $0 < s < 1$,

$$\sup_{\ell \in \mathbb{N}_0} (1 + |\mathcal{T}_\ell| - |\mathcal{T}_0|)^s (\mu(\mathcal{T}_\ell) + \eta_{\mathrm{S}}(\mathcal{T}_\ell)) \approx \sup_{N \in \mathbb{N}_0} (1+N)^s \min_{\mathcal{T} \in \mathbb{T}(N)} (\mu(\mathcal{T}) + \eta_{\mathrm{S}}(\mathcal{T})).$$

For the generalisation to higher-order polynomial degrees and inhomogeneous mixed boundary conditions in three spatial dimensions, the reader is referred to [37,64].

5. Numerical experiments

This section presents and compares the numerical results of NALSFEM, CALSFEM, and SALSFEM for three benchmark examples of the Poisson model problem and one of an elliptic problem with piecewise constant scalar diffusion constant. A primary focus consists of investigating the data approximation in Subsection 5.3 below. The lowest-order discretisation prevents any additional quadrature error for this benchmark problem.

5.1. Implementation and time measurement

The empirical investigation was carried out using the author's MATLAB software package octAFEM [65]. All experiments in this paper are reproducible with the compute capsule on the Code Ocean platform. The octAFEM package bases on the in-house MATLAB software package [66]. It was developed and tested under MATLAB version 9.14.0.2206163 (R2023a), but should be executable in older versions as well. Moreover, the code is completely compatible with the open-source software Octave (tested with version 8.1.0). The realisation differs from [37] because the object-oriented implementation therein employs a `Simplex` class for the representation of every simplex separately resulting in a huge computational overhead. Instead, the `ApproxTriangulation` in the implementation at hand includes an array of indices containing the complete history of simplices. The data approximation Algorithm 4 (AA) ensures linear complexity using binary bins as described in [62, Rem. 5.3]. It is incorporated into the `Triangulation` class from [37]. This allows the separate marking strategy in one triangulation object containing the complete refinement history of all simplices and thereby avoiding the computation of the overlay of $\mathcal{T}_{\mathrm{Tol}}$ and $\mathcal{T}_\ell$. The data error $\mu(T)$ of each simplex $T \in \mathcal{T}$ is stored in the array of `ApproxTriangulation` as well. It is computed when creating the simplex T. This causes some general overhead to the refinement process but may lead to some reduction of the runtime of AA because it can reuse information already created during a previous step of the NVB in a Case A of the separate marking algorithm.

The transformation formula allows to reduce the integral over any triangle to the reference triangle $T_{\mathrm{ref}} := \mathrm{conv}\{0,(1,0),(0,1)\}$. The transformation $\Phi : [0,1]^2 \to T_{\mathrm{ref}}$, $y \mapsto (y_1, (1-y_1)y_2)^{\mathsf{T}}$ from the unit square to the reference triangle shows

$$\int_{T_{\mathrm{ref}}} f \,\mathrm{d}x = \int_0^1 \int_0^1 (1-y_1)\, f(y_1, (1-y_1)y_2)\,\mathrm{d}y_2\,\mathrm{d}y_1.$$

The first integral with respect to y_2 is approximated by the Gauss–Legendre quadrature. The second integral with respect to y_1 employs the Gauss–Jacobi quadrature on the interval $[0,1]$ with weight function $w(\xi) = (1-\xi)$. Both one-dimensional quadrature nodes and weights are computed using the Golub–Welsch algorithm [67] with recursion coefficients from [68]. The resulting conical product rules with k^2 function evaluations, $k \in \mathbb{N}$, are exact for the integration of polynomials up to partial degree $2k-1$. For the evaluation of bilinear forms or integration of polynomial input data, the number of quadrature points is chosen such that the quadrature is exact.

The experiments investigating the performance of the algorithms in terms of the runtime are carried out with MATLAB version 9.9.0.1467703 (R2020b) on a compute server using 16 out of 128 Intel(R) Xeon(R) E7-8867 CPUs of 2.50 GHz and 2 TiB RAM. The code employs parallel computing for local quantities such as local stiffness matrices and the integration of the right-hand side. Since the MATLAB command `cputime` adds up the time for all parallel threads, the documentation recommends the measurement of real time. Additionally this exemplifies the practical performance as experienced by the user. To this end, time is measured on carefully selected parts of the program to distinguish the performance for the solution, estimation, and refinement. This allows to neglect possible overhead due to printing information to the command line or saving the results to disk. The time is measured in ten separate runs and averaged for improved reliability. The graphs below also indicate the maximal and the minimal measured time by vertical error bars to visualise possible inaccuracies of the measurement. The only significant differences occur for the very first iterations of each adaptive computation.

5.2. L-shaped domain

The Poisson model problem on the L-shaped domain $\Omega = (-1,1)^2 \setminus [0,1)^2$ with constant right-hand side $f \equiv 1$ is a standard benchmark for adaptive mesh refinement. The reentrant corner leads to reduced elliptic regularity of the unknown exact solution $u \in H^{1+s-\varepsilon}(\Omega)$ with $s = 2/3$ for all $\varepsilon > 0$. This is why uniform refinement exhibits a suboptimal convergence rate of $1/3$ with respect to the number of degrees of freedom (ndof) for the natural estimator η_{N} and the alternative estimator η_{C} in Fig. 2.

The convergence result in Theorem 4.5 asserts optimal rates for CALSFEM for sufficiently small bulk parameters $\theta < \theta_0$. The upper bound $\theta_0 = (1 + C_{\mathrm{stab}}^2 C_{\mathrm{drel}})^{-1}$ from [44, Prop. 4.2 (ii)] includes the generic constants of the stability and discrete reliability axiom. These constants are bounded in [69, Sect. 6] in the case of the Courant FEM on a mesh with right-isosceles triangles for the Poisson model problem by

$$C_{\mathrm{stab}}^2 \le 40.36 \quad \text{and} \quad C_{\mathrm{drel}} \le 9\,201. \tag{12}$$

This leads to the small theoretical lower bound of $\theta_0 \ge 2.6 \times 10^{-6}$. Nevertheless, Fig. 2b shows the optimal convergence rate already for moderate bulk parameters $\theta \le 0.8$ in practice.

The algorithm NALSFEM converges with the optimal rate for even larger bulk parameters $\theta \le 0.9$. The alternative estimator η_{C} focuses on the constitutive residual while the natural estimator η_{N} includes the equilibrium residual as well. This may explain the better performance of the natural refinement strategy for large bulk parameters. The difference is small and the coarse adaptively generated meshes look essentially identical for both refinement strategies as displayed in Fig. 3. A closer investigation of the fine triangulations with one million triangles and more exhibit an increased adaptive refinement towards the reentrant corner while at the same time allowing coarser triangles in

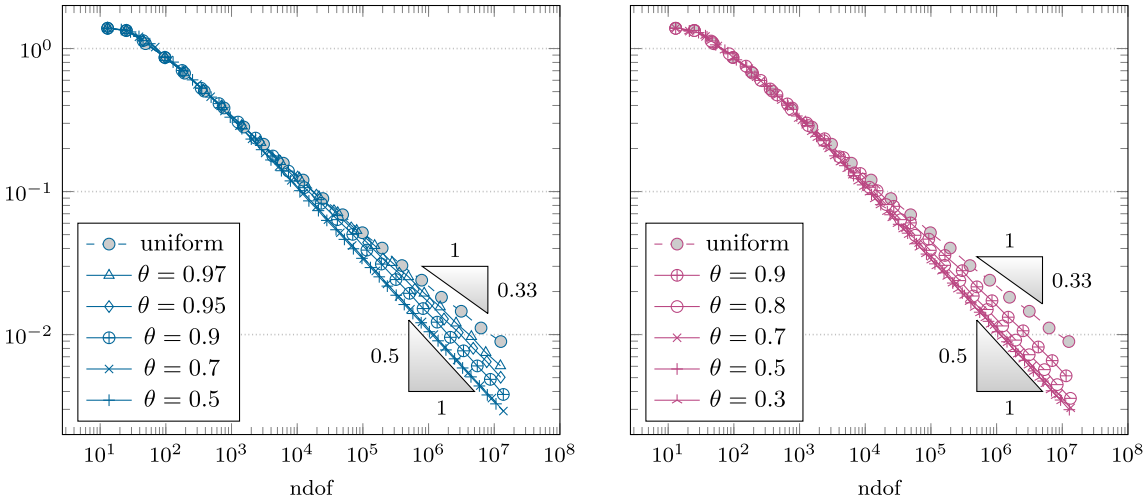

(a) Plot of $\eta_N(\mathcal{T}_\ell)$ in NALSFEM **(b)** Plot of $\eta_C(\mathcal{T}_\ell)$ in CALSFEM

Fig. 2. Comparison of various choices for the bulk parameter $0 < \theta \leq 1$ in the adaptive mesh-refinement strategies (uniform refinement for $\theta = 1$) for the benchmark problem on the L-shaped domain from Subsection 5.2.

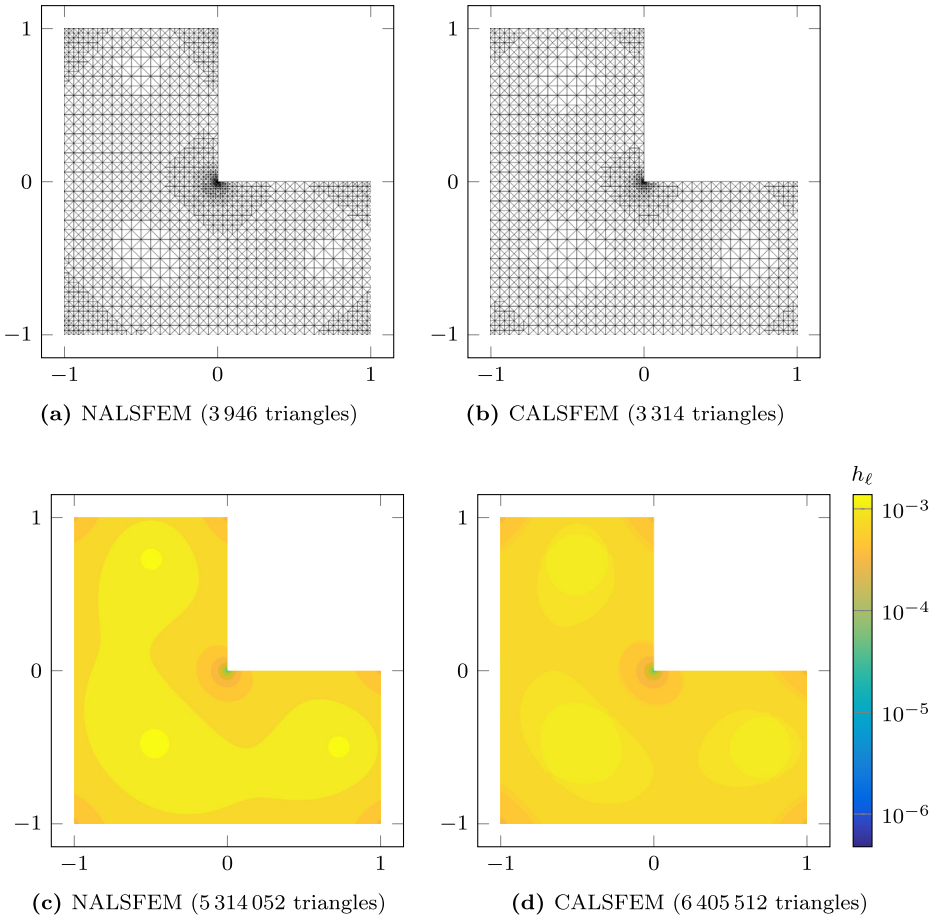

(a) NALSFEM (3 946 triangles) **(b)** CALSFEM (3 314 triangles)

(c) NALSFEM (5 314 052 triangles) **(d)** CALSFEM (6 405 512 triangles)

Fig. 3. Adaptively refined meshes from two different adaptive algorithms with bulk parameter $\theta = 0.9$ for the benchmark problem from Subsection 5.2. The Subfigures (c) and (d) display the mesh size $h_\ell|_T \equiv |T|^{1/2}$ for the triangles $T \in \mathcal{T}_\ell$ in a very fine triangulation. The same colour scale enables the comparison of the mesh size in the two algorithms.

the remaining parts of the domain for the NALSFEM compared to the CALSFEM.

Since the data f is resolved exactly on every triangulation $\mathcal{T} \in \mathbb{T}$, the data error and oscillation terms vanish $\mu(\mathcal{T}) = \operatorname{osc}(f, \mathcal{T}) = 0$. Hence,

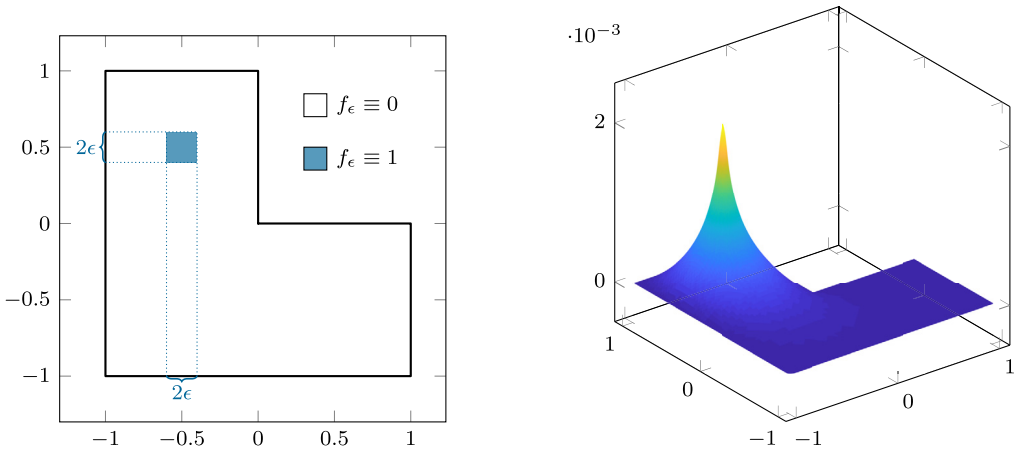

(a) Definition of right-hand side f_ϵ **(b)** Discrete solution u_ℓ for $\epsilon = 2^{-5}$

Fig. 4. Illustration of the microstructure in the benchmark problem from Subsection 5.3.

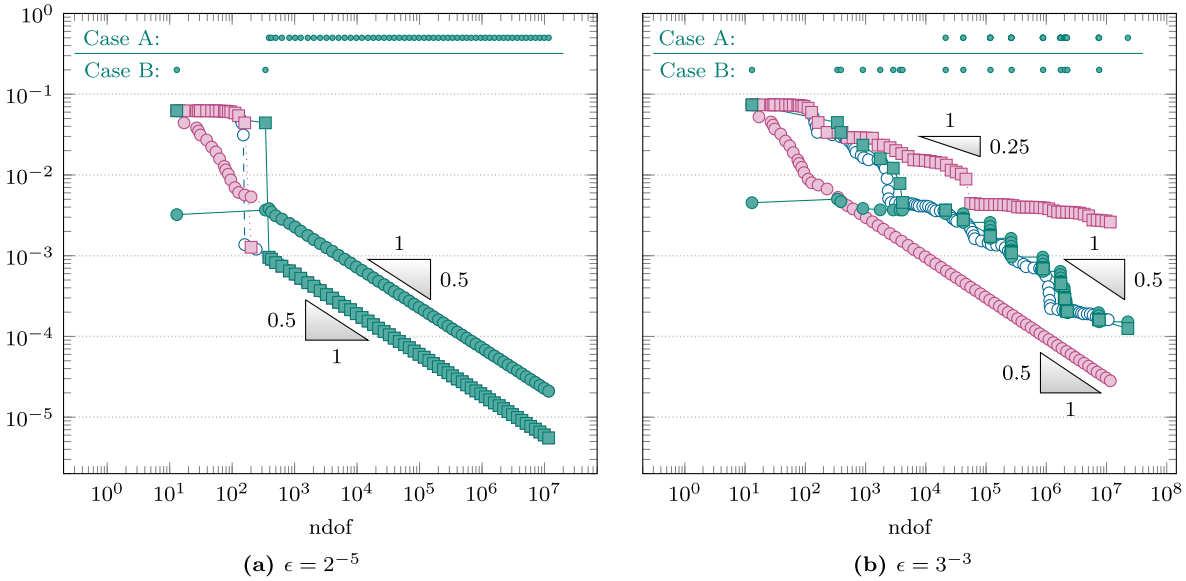

(a) $\epsilon = 2^{-5}$ **(b)** $\epsilon = 3^{-3}$

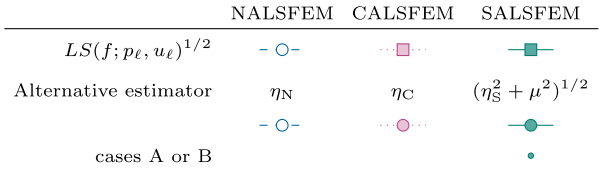

(c) Legend of Figures 5a–5b and 10

Fig. 5. Comparison of the three adaptive refinement strategies with parameters $\theta = 0.3$, $\kappa = 1$, and $\rho = 0.8$ for the solution of the benchmark problem from Subsection 5.3.

the case B in the separate marking does never hold and the SALSFEM algorithm provides exactly the same results as CALSFEM.

5.3. L-shaped domain with microstructure

The second benchmark considers the L-shaped domain $\Omega = (-1,1)^2 \setminus [0,1)^2$ from the Section 5.2 with a right-hand side $f_\epsilon \in L^2(\Omega)$ for some parameter $0 < \epsilon < 1/2$, given in [61, Sect. 3.4] by

$$f_\epsilon(x) := \begin{cases} 1, & \text{if } |x_1 + \tfrac{1}{2}| \le \epsilon \text{ and } |x_2 - \tfrac{1}{2}| \le \epsilon, \\ 0, & \text{otherwise.} \end{cases}$$

Fig. 4 illustrates the definition of f_ϵ and shows an example solution for $\epsilon = 2^{-5}$.

Due to the small support of the right-hand side f_ϵ, the quadrature described in Section 5.1 may be inaccurate, in particular for coarse triangulations. This is why the integration of the right-hand side for this benchmark is computed directly as the area of the convex intersection polygon of the support $\operatorname{supp}(f_\epsilon) = (-1/2-\epsilon, -1/2+\epsilon) \times (1/2-\epsilon, 1/2+\epsilon)$ and any triangle $T \in \mathcal{T}$. First, the vertices of the intersection polygon $x_1, \dots, x_J$ are determined by the Sutherland-Hodgman algorithm [70]. Second, the area of the intersection polygon is computed by the formula

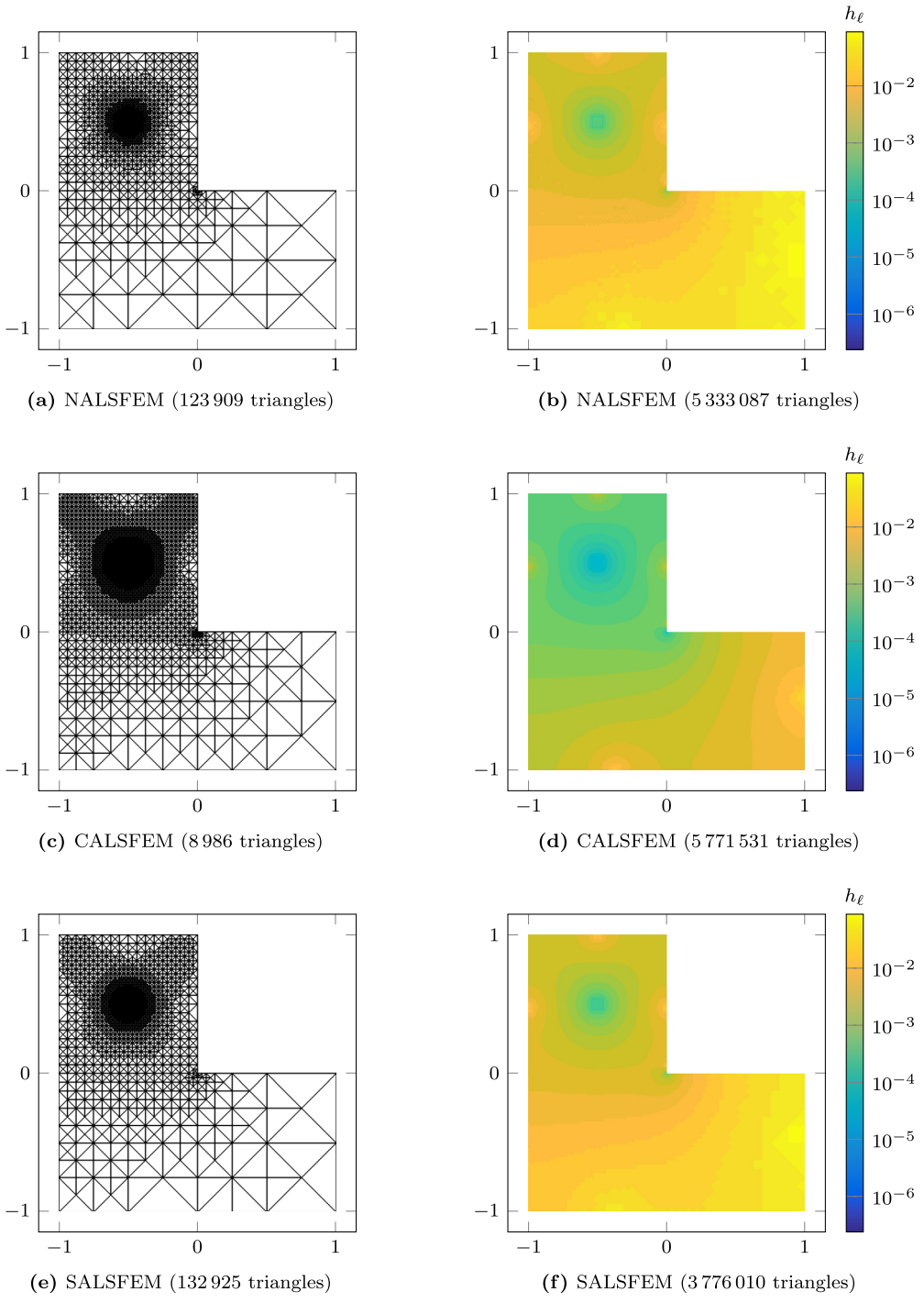

(a) NALSFEM (123 909 triangles) (b) NALSFEM (5 333 087 triangles)

(c) CALSFEM (8 986 triangles) (d) CALSFEM (5 771 531 triangles)

(e) SALSFEM (132 925 triangles) (f) SALSFEM (3 776 010 triangles)

Fig. 6. Adaptively generated meshes by the three refinement strategies with parameters $\theta = 0.3$, $\kappa = 1$, and $\rho = 0.8$ for the benchmark problem from Subsection 5.3 with $\epsilon = 3^{-3}$. The same colour scale enables the comparison of the mesh size $h_\ell|_T \equiv |T|^{1/2}$ for $T \in \mathcal{T}_\ell$ in the Subfigures (b), (d), and (f).

$$|\operatorname{supp}(f_\epsilon) \cap T| = \frac{1}{2}\Big|\sum_{j=1}^{J}(x_{j,1}x_{j+1,2} - x_{j,2}x_{j+1,1})\Big| \quad \text{with } x_{J+1} \equiv x_1.$$

This procedure allows for the exact computation of the piecewise constant approximation Πf_ϵ and the data error $\mu(\mathcal{T})$.

If the microstructure can be resolved exactly for $\epsilon = 2^{-m}$ with $m \in \mathbb{N}$, all three algorithms reach the point of exact data resolution and converge with the best possible rate from then on as displayed in Fig. 5a for $\epsilon = 2^{-5}$. Otherwise the data approximation plays a crucial role throughout the whole computation as for $\epsilon = 3^{-3}$ in Fig. 5b. For the algorithms NALSFEM and SALSFEM the least-squares functional converges with the optimal rate of 0.5. The indication of the cases at the top of the plot shows that the data approximation dominates in the first eight iterations of SALSFEM. The convergence behaviour of NALSFEM turns out to be very close to the separate marking algorithm but with significantly more intermediate solution steps. The alternative estimator η_C in CALSFEM converges with the optimal rate as well, as asserted by Theorem 4.5. However, it does not allow to control the data approximation as part of the divergence contribution to the error of the flux variable. This results in a suboptimal rate of 0.25 at the beginning of the computation when the data oscillation is presumably large enough. Once the dominance of the data approximation ends at about 5×10^4 degrees of freedom, the

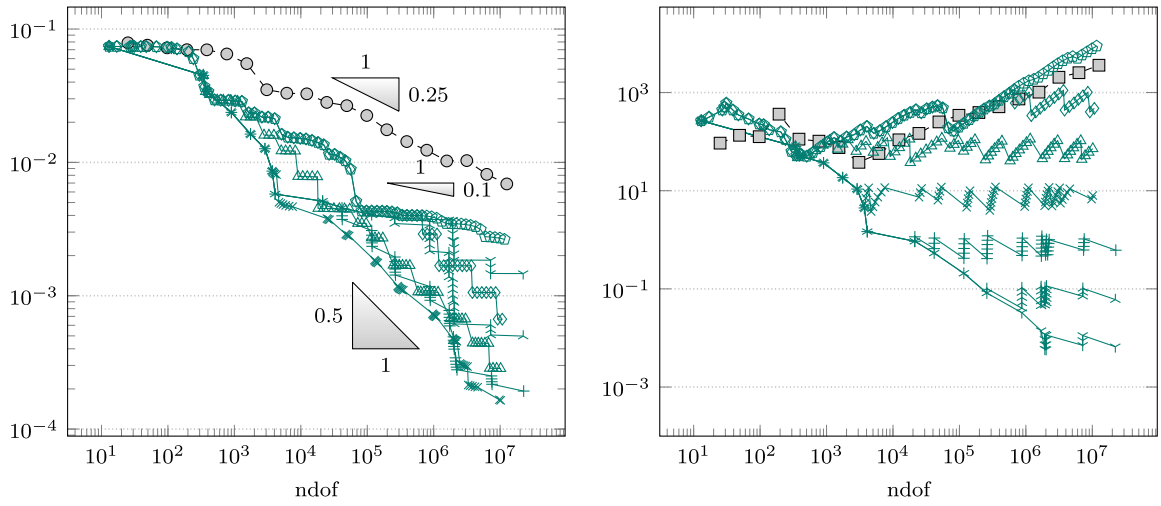

(a) Plot of estimator $(\eta_S^2(\mathcal{T}_\ell) + \mu^2(\mathcal{T}_\ell))^{1/2}$

(b) Plot of the quotient $q_\ell^2 := \mu^2(\mathcal{T}_\ell) / \eta_S^2(\mathcal{T}_\ell)$

(c) Legend for Figures 7a and 7b

Fig. 7. Comparison of various choices for the separation parameter $0 < \kappa$ in adaptive mesh refinement with SALSFEM for the benchmark problem from Subsection 5.3 with $\epsilon = 3^{-3}$.

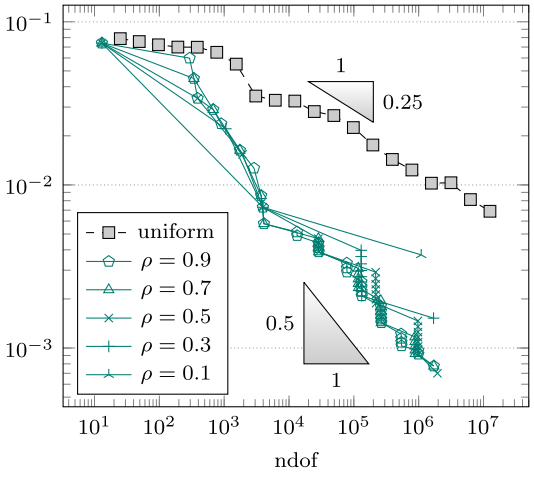

Fig. 8. Comparison of estimator $(\eta_S^2(\mathcal{T}_\ell) + \mu^2(\mathcal{T}_\ell))^{1/2}$ in SALSFEM for various parameters $0 < \rho < 1$ with $\theta = 0.3$ and $\kappa = 1$ for the benchmark problem from Subsection 5.3 with $\epsilon = 3^{-3}$.

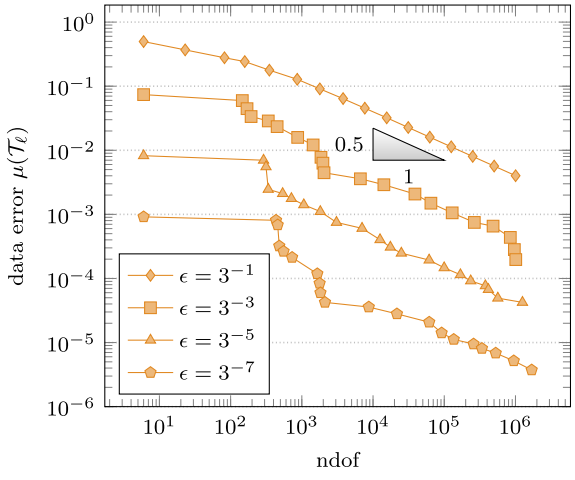

Fig. 9. Investigation of AA algorithm with $\rho = 0.9$ for the given data f_ϵ with varying microstructure parameter $0 < \epsilon < 1/2$ from Subsection 5.3.

CALSFEM algorithm is not able to considerably reduce the least-squares estimator any more.

The mesh plots in Fig. 6 demonstrate the different behaviour of the adaptive algorithms. The Figs. 6a, 6c, and 6e present the first level with an observable refinement towards the reentrant corner. While NALSFEM and SALSFEM focus on the microstructure up to more than 10^5 triangles, the CALSFEM already increases the refinement at the origin at about 7.4×10^3 triangles. The consideration of the very fine levels of more than 5.5×10^5 triangles exhibits a highly adaptive refinement at the boundary of the microstructure and the singularity at the reentrant corner. However, the mesh of the CALSFEM appears more uniformly with a larger minimal mesh size leading to the suboptimal convergence behaviour of the overall error as seen in the convergence history plot in Fig. 5b.

The convergence result in Theorem 4.6 requires the separation parameter $0 < \kappa < \kappa_0$ to be sufficiently small. The theoretical upper bound $\kappa_0 = \min\{\widetilde{\kappa}, C_{\mathrm{stab}}^{-2} C_{\mathrm{drel}}^{-1}\}$ from [38, Thm. 2.1] incorporates two conditions. If the data error $\mu(\mathcal{T})$ is monotonically decreasing under mesh refinement (i.e., $\Lambda_6 = 1$ in [38]), the estimator reduction in [38, Thm. 4.1] and thus the plain convergence in [38, Thm. 4.2] hold for arbitrary $0 < \kappa < \infty$. Hence, $\widetilde{\kappa} = \infty$. The proof of optimal convergence rates in [38, Sect. 4.3] requires $\kappa < C_{\mathrm{stab}}^{-2} C_{\mathrm{drel}}^{-1}$. The estimates (12) for the Courant FEM with right-isosceles triangles lead to $\kappa_0 \geq 2.6 \times 10^{-6}$. Despite this pessimistic theoretical bound, the convergence rate of SALSFEM is optimal for the large range of $10^{-2} \leq \kappa \leq 10^2$ in practice as displayed in Fig. 7a. This suggests that the algorithm is fairly robust to the choice of the parameter κ. Solely very large values exhibit suboptimal convergence rates. For $\kappa = 10^4$, every iteration carries out Case A with Dörfler marking for the alternative estimator. Hence, every larger value $\kappa \geq 10^4$ leads to exactly the same behaviour.

Fig. 7b displays the quotient $q_\ell^2 := \mu^2(\mathcal{T}_\ell)/\eta_S^2(\mathcal{T}_\ell)$ used for the decision of the refinement strategy in the separate marking. If this value is above the threshold κ, Case B holds and the data approximation algo-

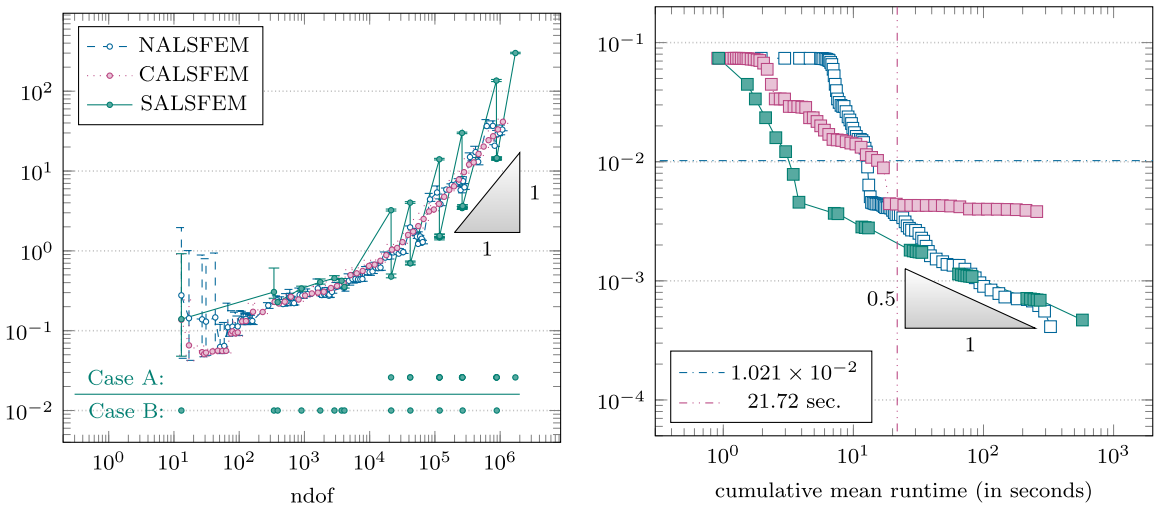

(a) Plot of mean total runtime (in seconds) **(b)** Plot of $LS(f; p_\ell, u_\ell)$

Fig. 10. Comparison of the three adaptive strategies with parameters $\theta = 0.3$, $\kappa = 1$, and $\rho = 0.8$ for the benchmark problem from Subsection 5.3 with $\epsilon = 3^{-3}$. Vertical error bars in Subfigure (a) indicate the maximal and minimal measured time. Both figures employ the markers and line styles as introduced by the legend in Fig. 5c.

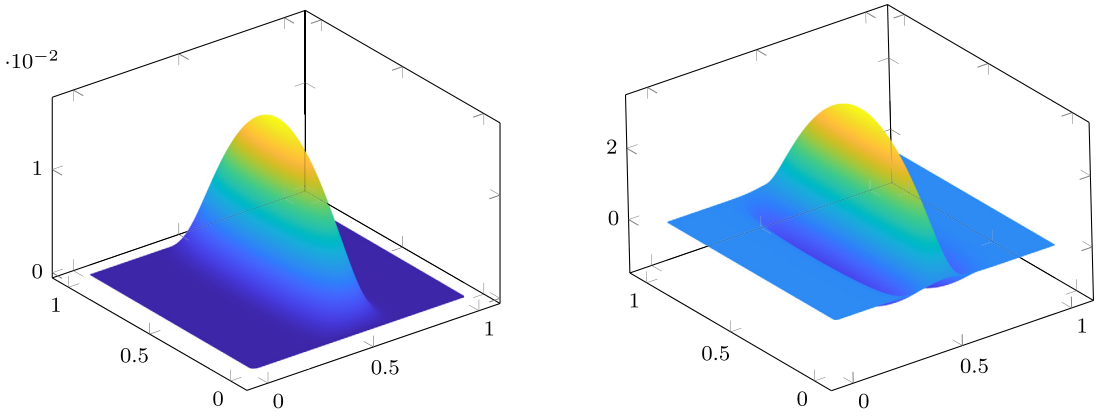

(a) Solution u **(b)** Right-hand side f

Fig. 11. Solution and right-hand side for the benchmark problem from Subsection 5.4.

rithm is carried out, otherwise in Case A, the Dörfler marking for the alternative estimator η_S and NVB apply. The reduction of η_S has rather no influence on the data error μ and, thus, leads to an increase of the quotient up to the threshold. This reveals that, throughout the computation, the SALSFEM algorithm ensures some balance of error estimator and data error specified by the parameter κ. For large quotients in the regime of the uniform refinement, solely Case A refinement is carried out leading to the highly suboptimal convergence rate of about 0.1 in Fig. 7a. This suggests a choice of κ considerably smaller than the values of the quotient q_ℓ^2 for uniform refinement.

As expected from the theoretical convergence result in Theorem 4.6, Fig. 8 approves that the choice of the parameter $0 < \rho < 1$ has no influence on the optimal convergence rate. However, the reduction of the parameter ρ decreases the number of solution steps significantly. While [71] suggests a relatively small ρ of about 0.1 for best overall performance, a value close to one allows a more sensitive behaviour in the distinction of the two refinement cases. Accordingly, the choice of $\rho = 0.8$ in the remaining experiments is preferable for an informative numerical comparison.

In order to investigate the performance of the three algorithms, Fig. 10a displays the mean total runtime in each iteration from 10 independent runs of the adaptive loop. All three refinement algorithms exhibit almost linear complexity with respect to the number of degrees of freedom. Note that the direct solution of the algebraic linear system prevents linear complexity of the overall implementation at hand.

The plot in Fig. 10b displaying the estimator values versus the cumulative mean runtime instead of the number of degrees of freedom better represents the practical performance. The adaptive algorithms ran up to 10^5 degrees of freedom. In particular for the beginning of the computation the SALSFEM is superior to the other refinement strategies. This is because of the reduced number of solution steps which may be further decreased by reducing the parameter ρ. Later NALSFEM and SALSFEM provide comparable results.

As a reference, Fig. 10b displays the value $LS(f; p_\ell, u_\ell) \approx 1.02110264 \times 10^{-2}$ resulting from a computation of a fine uniform mesh with 786 432 triangles (`ndof` = 1 572 865). The solution and estimation took an average runtime of about 21.72 seconds (without considering the time for the generation of the fine mesh and the computation of the alternative estimators). The SALSFEM algorithm achieves the same accuracy already after 3 seconds. NALSFEM and even CALSFEM reach this threshold after approximately 10 seconds although the latter does not guarantee any control of the data approximation error. This is another striking evidence of the superiority of adaptive mesh-refinement algorithms.

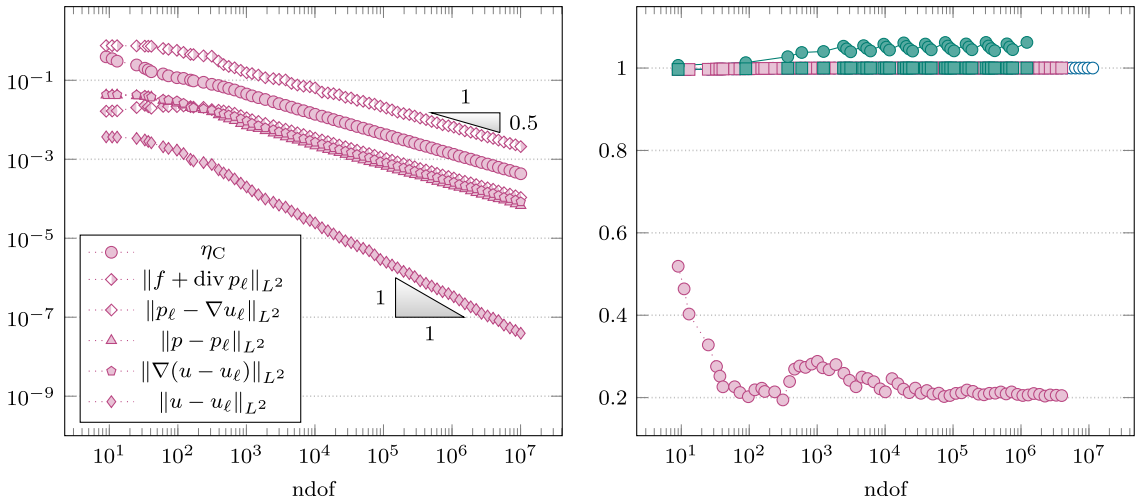

(a) Plot of estimators and errors in CALSFEM

(b) Plot of efficiency indices

	NALSFEM	CALSFEM	SALSFEM
$LS(f;p_\ell,u_\ell)^{1/2}/e_\ell$	– ○ –	···□···	—■—
Alternative estimator	η_N/e_ℓ	η_C/e_ℓ	$(\eta_S^2+\mu^2)^{1/2}/e_\ell$
	– ○ –	···●···	—●—

(c) Legend of Figure 12b and 16b

Fig. 12. Convergence history plot and plot of the efficiency indices with respect to the error $e_\ell := |||(p-p_\ell, u-u_\ell)|||$ for the waterfall benchmark problem from Subsection 5.4. The parameters for the adaptive mesh-refinement strategies read $\theta = 0.3$, $\kappa = 1$, and $\rho = 0.8$.

Finally, Fig. 9 confirms the quasi-optimality of the AA algorithm [38, axiom (B1) in Sect. 2.4] with respect to the number of degrees of freedom.

5.4. Waterfall benchmark

This benchmark considers the exact solution $u \in H^1_0(\Omega)$ on the unit square $\Omega := (0,1)^2$ given in [72, Sect. 4.2] by

$$u(x) := x_1(x_1-1)x_2(x_2-1)\exp\big(-100(x_1-1/2)^2-(x_2-117)^2/10000\big).$$

The right-hand side is determined by $f := -\Delta u$. Both functions are displayed in Fig. 11.

For this benchmark with a smooth solution, all adaptive algorithms exhibit optimal convergence rates with a relatively small pre-asymptotic range. Exemplarily, Fig. 12a presents the convergence graphs for the CALSFEM. It confirms the equivalence of the estimator with the exact error terms. It is remarkable that even the data error $\mu^2(\mathcal{T}_\ell) \le \|f + \operatorname{div} p_\ell\|^2_{L^2(\Omega)}$ converges with the optimal rate, although this is not guaranteed by the theoretical convergence result. Fig. 12b displays the efficiency indices of all three mesh-refinement schemes. The results illustrate the exactness of the built-in error estimator $LS(f;p_\ell,u_\ell)^{1/2}$ from Theorem 4.1 already on the coarsest triangulations. This is because the term $\|f + \operatorname{div} p_\ell\|_{L^2(\Omega)} = \|\operatorname{div}(p-p_\ell)\|_{L^2(\Omega)}$ dominates from the very beginning in Fig. 12a and belongs to the built-in error estimator $LS(f;p_\ell,u_\ell)^{1/2}$ and the error $e_\ell := |||(p-p_\ell,u-u_\ell)|||$ as well. The fact that this dominating term is not controlled by the alternative estimator η_C explains why the latter attains low efficiency indices only.

The mesh plots in Fig. 13 illustrate the different behaviour of the adaptive algorithms. The NALSFEM in Fig. 13a focusses on the regions with large gradients of the right-hand side f (see Fig. 11b) in order to allow for a proper piecewise constant approximation. The mesh is similar to the result from the data approximation by AA in Fig. 13d. On the contrary, the CALSFEM in Fig. 13b increases the refinement in regions with large absolute values of f. The SALSFEM in Fig. 13c seemingly combines both aspects.

5.5. Discontinuous coefficients

The final benchmark considers the elliptic problem with piecewise constant scalar diffusion coefficient $a \in L^\infty(\Omega)$, defined by

$$a(x) := \begin{cases} a_1 & \text{if } 0 < x_1x_2, \\ a_2 & \text{if } x_1x_2 < 0, \end{cases}$$

and right-hand side $f \equiv 0$ on the square domain $\Omega := (-1,1)^2$. It seeks $(p,u) \in H(\operatorname{div},\Omega) \times H^1(\Omega)$ satisfying

$$f + \operatorname{div} p = 0 \quad \text{and} \quad a^{-1/2}p - a^{1/2}\nabla u = 0 \quad \text{in } \Omega \quad \text{subject to}$$
$$u = u_D \text{ on } \partial\Omega. \tag{13}$$

The weighting of the second residual in (13) leads to the fundamental equivalence of the least-squares functional

$$LS(f,a;p,u) := \|f + \operatorname{div} p\|^2_{L^2(\Omega)} + \|a^{-1/2}p - a^{1/2}\nabla u\|^2_{L^2(\Omega)} \tag{14}$$

and the natural weighted $H(\operatorname{div})$ and energy norm $\|\operatorname{div} q\|^2_{L^2(\Omega)} + \|a^{-1/2}q\|^2_{L^2(\Omega)} + \|a^{1/2}\nabla u\|^2_{L^2(\Omega)}$ with equivalence constants solely depending on the uniform lower bound of the diffusion coefficient. Note that the inhomogeneous Dirichlet boundary conditions u_D lead to an additional oscillation term in the estimators η_N, η_C, and η_S [35,37,40] and the overall error

$$|||(q,v)|||^2_a := \|\operatorname{div} q\|^2_{L^2(\Omega)} + \|a^{-1/2}q\|^2_{L^2(\Omega)} + \|a^{1/2}\nabla u\|^2_{L^2(\Omega)} + \sum_{E\in\mathcal{E}(\partial\Omega)} |\omega_E|^{1/2}\|(1-\Pi_{0,E})\partial u_D/\partial s\|^2_{L^2(E)}. \tag{15}$$

For some parameter $0 < \gamma < 2$, the exact weak solution to (13) in polar coordinates from [73] reads $u(r,\phi) := r^\gamma \mu(\phi)$ and $p := a\nabla u$ with

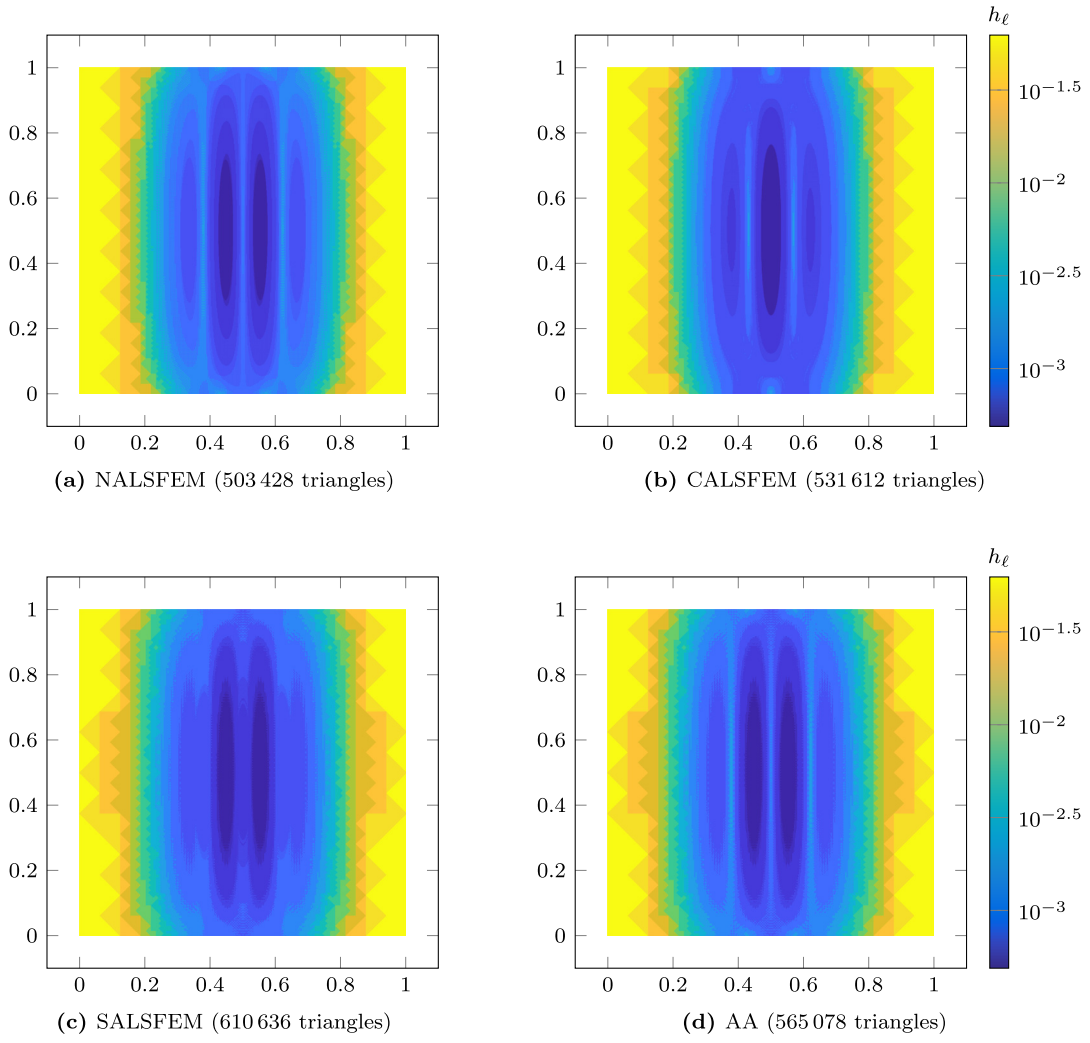

(a) NALSFEM (503 428 triangles) **(b)** CALSFEM (531 612 triangles)

(c) SALSFEM (610 636 triangles) **(d)** AA (565 078 triangles)

Fig. 13. Plots of adaptively refined meshes for the three refinement strategies with parameters $\theta = 0.3$, $\kappa = 10$, and $\rho = 0.8$ for the benchmark problem from Subsection 5.4.

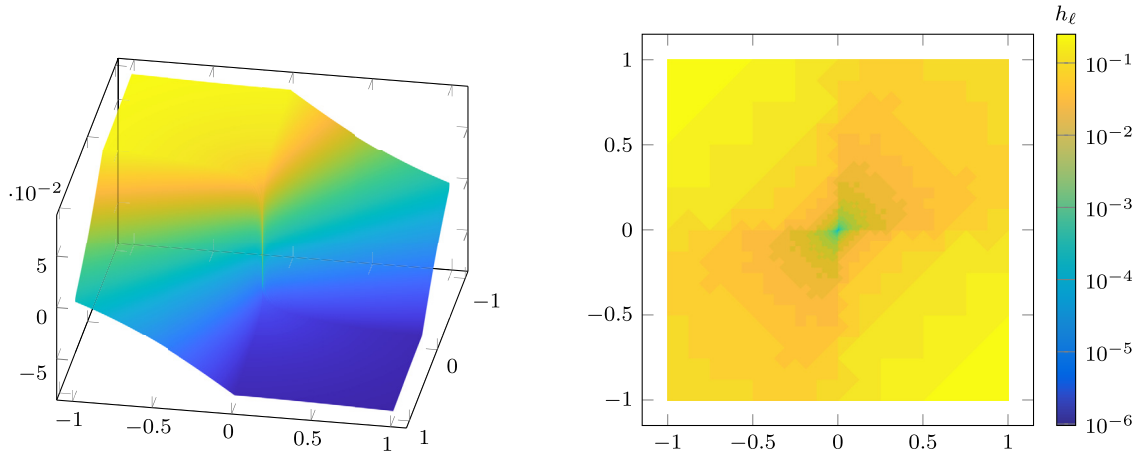

(a) Solution u **(b)** CALSFEM (5 370 triangles)

Fig. 14. Solution plot and plot of mesh size $h_\ell|_T \equiv |T|^{1/2}$ of adaptively refined mesh using CALSFEM with bulk parameter $\theta = 0.7$ for the benchmark problem from Subsection 5.5.

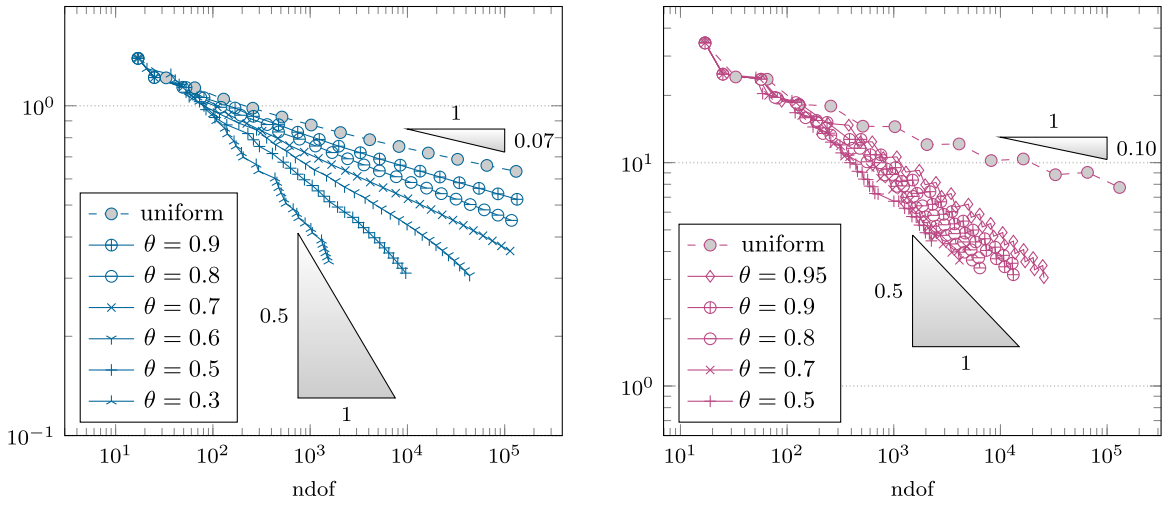

(a) Plot of $\eta_N(\mathcal{T}_\ell)$ in NALSFEM **(b)** Plot of $\eta_C(\mathcal{T}_\ell)$ in CALSFEM

Fig. 15. Comparison of various choices for the bulk parameter $0 < \theta \leq 1$ in the adaptive mesh-refinement strategies for the benchmark problem from Subsection 5.5.

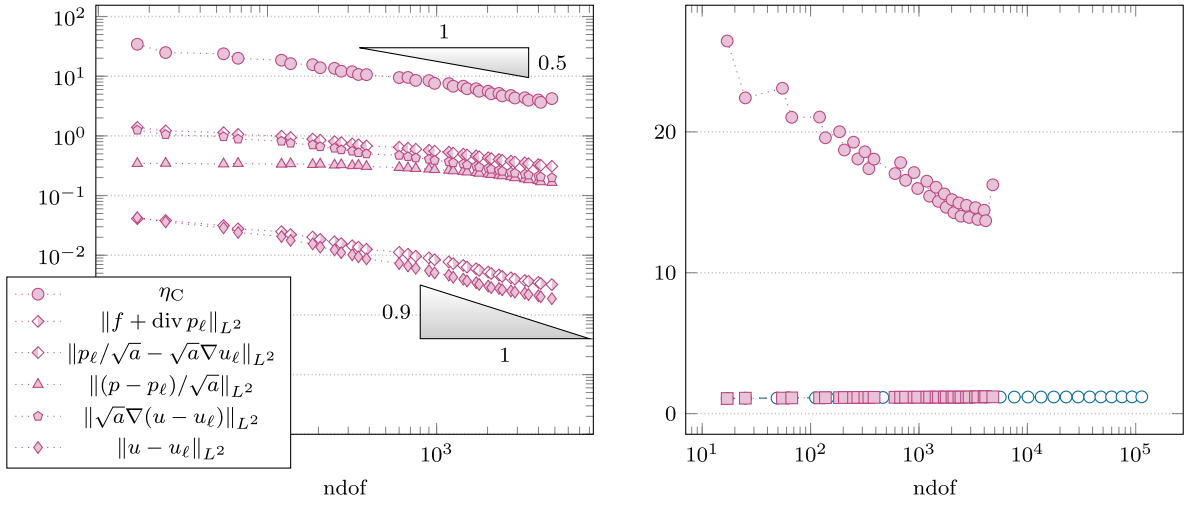

(a) Plot of errors and estimators in CALSFEM **(b)** Plot of efficiency indices

Fig. 16. Convergence history plot of CALSFEM with bulk parameter $\theta = 0.7$ and efficiency indices with respect to the error $e_\ell := |||(p - p_\ell, u - u_\ell)|||_a$ from (15) for the diffusion benchmark problem from Subsection 5.5. Fig. 16b employs the graphs as introduced by the legend in Fig. 12c.

$$\mu(\phi) := \begin{cases} \cos((\pi/2-\sigma)\gamma)\cos((\phi-\pi/2+\rho)\gamma) & \text{if } 0 \leq \phi < \pi/2, \\ \cos(\rho\gamma)\cos((\phi-\pi+\sigma)\gamma) & \text{if } \pi/2 \leq \phi < \pi, \\ \cos(\sigma\gamma)\cos((\phi-\pi-\rho)\gamma) & \text{if } \pi \leq \phi < 3\pi/2, \\ \cos((\pi/2-\rho)\gamma)\cos((\phi-3\pi/2-\sigma)\gamma) & \text{if } 3\pi/2 \leq \phi \leq 2\pi, \end{cases}$$

and constants $0 < \rho$ and $\sigma < 0$. The parameter γ determines the regularity of the solution $u \in H^{1+\gamma-\varepsilon}(\Omega)$ for all $0 < \varepsilon$. The choice of $\gamma = 0.1$ in [74] leads to the constants $\rho = \pi/4$, $\sigma \approx -14.922\,565\,104\,551\,52$, the coefficients $a_1 \approx 161.447\,638\,797\,588\,1$, $a_2 = 1$, and the solution u displayed in Fig. 14a. The nodal interpolation of the exact solution u prescribes the inhomogeneous boundary conditions u_D in the discrete minimization of (14).

This benchmark problem models intersecting interfaces with the difficulty of a strong cross-point singularity at the origin. Fig. 14b exhibits the intense adaptive refinement of CALSFEM towards the origin. The heavy grading of the mesh leads to ill-conditioned system matrices already for a relatively small number of degrees of freedom, e.g., from about `ndof` $= 4\,000$ for CALSFEM with $\theta = 0.7$. For this reason, its unreliable results are omitted in the figures. Moreover, due to the lack of any data approximation error for the right-hand side f, the results of CALSFEM and SALSFEM coincide.

The plain convergence analysis for NALSFEM from Theorem 4.2 holds under general assumptions. However, the convergence result in [42] requires nested discrete spaces which is violated by the nodal interpolation of the boundary data in the implementation at hand. The analysis in [24] covers inhomogeneous boundary conditions if they are weakly enforced by additional residuals in the least-squares functional. Nevertheless, NALSFEM converges for all choices of the bulk parameter in Fig. 15a. In contrast to Fig. 2a for the L-shaped domain benchmark, the convergence of NALSFEM with the optimal rate seems to require much smaller bulk parameters $\theta \leq 0.3$ in this benchmark problem. In contrast to that, CALSFEM appears to be much more robust with respect to the choice of $0 < \theta \leq 1$ in Fig. 15b.

The case of piecewise constant diffusion coefficient is included in the analysis of [37]. Hence, Theorem 4.6 for the optimal convergence rates of SALSFEM (and so of CALSFEM) generalises to the elliptic problem (13) as well. Fig. 16a confirms the optimal convergence rates even for a rather large bulk parameter $\theta = 0.7$. The efficiency indices of the

built-in error estimator $LS(f;p_\ell,u_\ell)^{1/2}$ range from 1 to 1.25 in Fig. 16b providing further empirical evidence for its accurate error estimation properties. The slight increase of these indices might result from the approximation of inhomogeneous Dirichlet boundary conditions which are not covered by [29].

6. Conclusion and open questions

The numerical experiments show that the adaptive algorithm with separate marking is superior in particular on moderate levels and for obtaining an overall high accuracy. However, the realisation of the separate marking and of the data approximation algorithm is more involved and usually not included in standard FEM software packages. Since the natural mesh refinement leads to comparable results as the separate marking algorithm, it is a good alternative. The investigation of the efficiency indices confirmed the exactness of the built-in error estimator even on coarse meshes.

Choices of moderate bulk parameters of $0.3 \le \theta \le 0.5$ provide optimal convergence rates while still ensuring a tolerable number of solution steps. The investigation of the separation parameter κ in Subsection 5.3 suggests a choice of κ of one order of magnitude less than the quotient $q_\ell^2 = \mu^2(\mathcal{T}_\ell)/\eta_S^2(\mathcal{T}_\ell)$ in the case of uniform refinement. The evaluation of q_ℓ for $\ell = 0$ or small levels $\ell > 0$ allow for a justified a priori choice of κ. The convergence rate is robust with respect to the parameter ρ. Smaller values of ρ significantly reduce the number of solution steps while larger values enable the adaptive algorithm to balance error estimator reduction and data approximation more accurately.

The adaptive LSFEM is well-established and convincing in many applications. However, important mathematical questions remain open. The proof of Theorem 4.3 on Q-linear convergence of the natural adaptive LSFEM heavily relies on the lowest-order arguments such that a straight-forward generalisation to higher polynomial degrees seems inaccessible. Additionally, the restriction to sufficiently large bulk parameters appears artificial and the case of small θ is not covered yet. Once this has been solved, the linear convergence would imply optimal convergence rates with respect to the number of degrees of freedom by Theorem 4.4. Moreover, the study of optimal convergence rates with respect to the computational costs in the spirit of [41] represents an important task for future research. While the collective marking algorithm fits into the framework of [41], the application to an adaptive algorithm with separate marking and data approximation requires a major modification as for the axioms of adaptivity in [38].

Data availability

The software package octAFEM for the numerical experiments has been published on the Code Ocean platform under the DOI 10.24433/CO.6310426.v1.

Link to the Reproducible Capsule

https://doi.org/10.24433/CO.6310426.v1

References

[1] B.-N. Jiang, G.F. Carey, Adaptive refinement for least-squares finite elements with element-by-element conjugate gradient solution, Int. J. Numer. Methods Eng. 24 (3) (1987) 569–580, https://onlinelibrary.wiley.com/doi/abs/10.1002/nme.1620240308.

[2] M. Berndt, T.A. Manteuffel, S.F. McCormick, Local error estimates and adaptive refinement for first-order system least squares (FOSLS), in: Special Issue on Multilevel Methods, Copper Mountain, CO, 1997, Electron. Trans. Numer. Anal. 6 (Dec. 1997) 35–43.

[3] J.-L. Liu, Exact a posteriori error analysis of the least squares finite element method, Appl. Math. Comput. 116 (3) (2000) 297–305, https://doi.org/10.1016/S0096-3003(99)00153-8.

[4] T. Führer, N. Heuer, M. Karkulik, MINRES for second-order PDEs with singular data, SIAM J. Numer. Anal. 60 (3) (2022) 1111–1135, https://doi.org/10.1137/21M1457023.

[5] J. Ku, E.-J. Park, A posteriori error estimators for the first-order least-squares finite element method, J. Comput. Appl. Math. 235 (1) (2010) 293–300.

[6] J.H. Adler, T.A. Manteuffel, S.F. McCormick, J.W. Nolting, J.W. Ruge, L. Tang, Efficiency based adaptive local refinement for first-order system least-squares formulations, SIAM J. Sci. Comput. 33 (1) (2011) 1–24.

[7] M. Brezina, J. Garcia, T. Manteuffel, S. McCormick, J. Ruge, L. Tang, Parallel adaptive mesh refinement for first-order system least squares, Numer. Linear Algebra Appl. 19 (2) (2012) 343–366, https://doi.org/10.1002/nla.1820.

[8] G. Starke, A first-order system least squares finite element method for the shallow water equations, SIAM J. Numer. Anal. 42 (6) (2005) 2387–2407, https://doi.org/10.1137/S0036142903438124.

[9] G. Danisch, Gemischte Finite Elemente Least-Squares Methoden für die Flachwassergleichung mit kleiner Viskosität (Mixed least-squares finite element method for the shallow water equation with small viscosity) (in German), PhD thesis, Gottfried Wilhelm Leibniz Universität Hannover, 2007.

[10] S. Münzenmaier, G. Starke, First-order system least squares for coupled Stokes-Darcy flow, SIAM J. Numer. Anal. 49 (1) (2011) 387–404, https://doi.org/10.1137/100805108.

[11] S. Münzenmaier, First-order system least squares for generalized-Newtonian coupled Stokes-Darcy flow, Numer. Methods Partial Differ. Equ. 31 (4) (2015) 1150–1173, https://doi.org/10.1002/num.21939.

[12] Z. Cai, C. Westphal, An adaptive mixed least-squares finite element method for viscoelastic fluids of Oldroyd type, J. Non-Newton. Fluid Mech. 159 (1) (2009) 72–80, https://www.sciencedirect.com/science/article/pii/S0377025709000366.

[13] F. Bertrand, First-order system least-squares for interface problems, SIAM J. Numer. Anal. 56 (3) (2018) 1711–1730, https://doi.org/10.1137/16M1105827.

[14] O. Kayser-Herold, Least-Squares Methods for the Solution of Fluid-Structure Interaction Problems, PhD thesis, Technische Universität Braunschweig, 2006.

[15] Z. Cai, J. Korsawe, G. Starke, An adaptive least squares mixed finite element method for the stress-displacement formulation of linear elasticity, Numer. Methods Partial Differ. Equ. 21 (1) (2005) 132–148.

[16] Z. Cai, G. Starke, Least-squares methods for linear elasticity, SIAM J. Numer. Anal. 42 (2) (2004) 826–842.

[17] G. Starke, An adaptive least-squares mixed finite element method for elasto-plasticity, SIAM J. Numer. Anal. 45 (1) (2007) 371–388.

[18] F.S. Attia, Z. Cai, G. Starke, First-order system least squares for the Signorini contact problem in linear elasticity, SIAM J. Numer. Anal. 47 (4) (2009) 3027–3043, https://doi.org/10.1137/080726975.

[19] R. Krause, B. Müller, G. Starke, An adaptive least-squares mixed finite element method for the Signorini problem, Numer. Methods Partial Differ. Equ. 33 (1) (2017) 276–289, https://doi.org/10.1002/num.22086.

[20] J.M. Fiard, T.A. Manteuffel, S.F. McCormick, First-order system least squares (FOSLS) for convection-diffusion problems: numerical results, SIAM J. Sci. Comput. 19 (6) (1998) 1958–1979, https://doi.org/10.1137/S1064827596301169.

[21] M. Majidi, G. Starke, Least-squares Galerkin methods for parabolic problems. II. The fully discrete case and adaptive algorithms, SIAM J. Numer. Anal. 39 (5) (2001/2002) 1648–1666, https://doi.org/10.1137/S0036142900379461.

[22] H. Gu, H. Li, An adaptive least-squares mixed finite element method for nonlinear parabolic problems, Comput. Math. Model. 20 (2) (2009) 192–206, https://doi.org/10.1007/s10598-009-9028-z.

[23] T. Führer, M. Karkulik, Space-time least-squares finite elements for parabolic equations, Comput. Math. Appl. 92 (2021) 27–36, https://doi.org/10.1016/j.camwa.2021.03.004.

[24] G. Gantner, R. Stevenson, Further results on a space-time FOSLS formulation of parabolic PDEs, ESAIM: Math. Model. Numer. Anal. 55 (1) (2021) 283–299.

[25] L.N. Olson, Multilevel Least-Squares Finite Element Methods for Hyperbolic Partial Differential Equations, PhD thesis, University of Colorado, 2003.

[26] Q. Liu, S. Zhang, Adaptive least-squares finite element methods for linear transport equations based on an H(div) flux reformulation, Comput. Methods Appl. Mech. Eng. 366 (2020) 113041, https://doi.org/10.1016/j.cma.2020.113041.

[27] Q. Liu, S. Zhang, Adaptive flux-only least-squares finite element methods for linear transport equations, J. Sci. Comput. 84 (2) (2020) 26, https://doi.org/10.1007/s10915-020-01269-y.

[28] J.H. Chaudhry, S.D. Bond, L.N. Olson, A weighted adaptive least-squares finite element method for the Poisson-Boltzmann equation, Appl. Math. Comput. 218 (9) (2012) 4892–4902, https://doi.org/10.1016/j.amc.2011.10.054.

[29] C. Carstensen, J. Storn, Asymptotic exactness of the least-squares finite element residual, SIAM J. Numer. Anal. 56 (4) (2018) 2008–2028.

[30] P. Bringmann, C. Carstensen, N.T. Tran, Adaptive least-squares, discontinuous Petrov-Galerkin, and hybrid high-order methods, in: Non-standard Discretisation Methods in Solid Mechanics, in: Lect. Notes Appl. Comput. Mech., vol. 98, Springer, Cham, 2022, pp. 107–147.

[31] W. Qiu, S. Zhang, Adaptive first-order system least-squares finite element methods for second-order elliptic equations in nondivergence form, SIAM J. Numer. Anal. 58 (6) (2020) 3286–3308, https://doi.org/10.1137/19M1271099.

[32] T. Führer, First-order least-squares method for the obstacle problem, Numer. Math. 144 (1) (2020) 55–88, https://doi.org/10.1007/s00211-019-01084-0.

[33] C. Carstensen, E.-J. Park, Convergence and optimality of adaptive least squares finite element methods, SIAM J. Numer. Anal. 53 (1) (2015) 43–62.

[34] P. Bringmann, C. Carstensen, An adaptive least-squares FEM for the Stokes equations with optimal convergence rates, Numer. Math. 135 (2) (2017) 459–492.

[35] P. Bringmann, C. Carstensen, h-adaptive least-squares finite element methods for the 2D Stokes equations of any order with optimal convergence rates, Comput. Math. Appl. 74 (8) (2017) 1923–1939.
[36] P. Bringmann, C. Carstensen, G. Starke, An adaptive least-squares FEM for linear elasticity with optimal convergence rates, SIAM J. Numer. Anal. 56 (1) (2018) 428–447.
[37] P. Bringmann, Adaptive least-squares finite element method with optimal convergence rates, PhD thesis, Humboldt-Universität zu Berlin, 2021.
[38] C. Carstensen, H. Rabus, Axioms of adaptivity with separate marking for data resolution, SIAM J. Numer. Anal. 55 (6) (2017) 2644–2665.
[39] C. Carstensen, Collective marking for adaptive least-squares finite element methods with optimal rates, Math. Comput. 89 (321) (2020) 89–103.
[40] C. Carstensen, R. Ma, Collective marking for arbitrary order adaptive least-squares finite element methods with optimal rates, Comput. Math. Appl. 95 (2021) 271–281.
[41] G. Gantner, A. Haberl, D. Praetorius, S. Schimanko, Rate optimality of adaptive finite element methods with respect to overall computational costs, Math. Comput. 90 (331) (2021) 2011–2040.
[42] T. Führer, D. Praetorius, A short note on plain convergence of adaptive least-squares finite element methods, Comput. Math. Appl. 80 (6) (2020) 1619–1632.
[43] C. Carstensen, E.-J. Park, P. Bringmann, Convergence of natural adaptive least squares finite element methods, Numer. Math. 136 (4) (2017) 1097–1115.
[44] C. Carstensen, M. Feischl, M. Page, D. Praetorius, Axioms of adaptivity, Comput. Math. Appl. 67 (6) (2014) 1195–1253.
[45] R. Stevenson, The completion of locally refined simplicial partitions created by bisection, Math. Comput. 77 (261) (2008) 227–241.
[46] M. Karkulik, D. Pavlicek, D. Praetorius, On 2D newest vertex bisection: optimality of mesh-closure and H^1-stability of L_2-projection, Constr. Approx. 38 (2) (2013) 213–234.
[47] J.M. Maubach, Local bisection refinement for n-simplicial grids generated by reflection, SIAM J. Sci. Comput. 16 (1) (1995) 210–227.
[48] I. Kossaczký, A recursive approach to local mesh refinement in two and three dimensions, J. Comput. Appl. Math. 55 (3) (1994) 275–288.
[49] C.T. Traxler, An algorithm for adaptive mesh refinement in n dimensions, Computing 59 (2) (1997) 115–137.
[50] W. Dörfler, A convergent adaptive algorithm for Poisson's equation, SIAM J. Numer. Anal. 33 (3) (1996) 1106–1124.
[51] C.-M. Pfeiler, D. Praetorius, Dörfler marking with minimal cardinality is a linear complexity problem, Math. Comput. 89 (326) (2020) 2735–2752.
[52] D.C. Jespersen, A least squares decomposition method for solving elliptic equations, Math. Comput. 31 (140) (1977) 873–880, https://doi.org/10.2307/2006118.
[53] Z. Cai, V. Carey, J. Ku, E.-J. Park, Asymptotically exact a posteriori error estimators for first-order div least-squares methods in local and global L_2 norm, Comput. Math. Appl. 70 (4) (2015) 648–659.
[54] J. Ku, Local error estimates for least-squares finite element methods for first-order system, J. Comput. Appl. Math. 299 (2016) 92–100, https://doi.org/10.1016/j.cam.2015.10.029.
[55] K.G. Siebert, A convergence proof for adaptive finite elements without lower bound, IMA J. Numer. Anal. 31 (3) (2011) 947–970.
[56] R. Stevenson, Optimality of a standard adaptive finite element method, Found. Comput. Math. 7 (2) (2007) 245–269.
[57] J.M. Cascon, C. Kreuzer, R.H. Nochetto, K.G. Siebert, Quasi-optimal convergence rate for an adaptive finite element method, SIAM J. Numer. Anal. 46 (5) (2008) 2524–2550.
[58] T. Manteuffel, S. McCormick, J. Nolting, J. Ruge, G. Sanders, Further results on error estimators for local refinement with first-order system least squares (FOSLS), Numer. Linear Algebra Appl. 17 (2–3) (2010) 387–413, https://doi.org/10.1002/nla.696.
[59] F. Bertrand, D. Boffi, First order least-squares formulations for eigenvalue problems, IMA J. Numer. Anal. 42 (2) (2022) 1339–1363, https://doi.org/10.1093/imanum/drab005.
[60] C. Carstensen, H. Rabus, An optimal adaptive mixed finite element method, Math. Comput. 80 (274) (2011) 649–667.
[61] H. Rabus, Quasi-optimal convergence of AFEM based on separate marking, Part I and II, J. Numer. Math. 23 (2) (2015) 137–156.
[62] P. Binev, R. DeVore, Fast computation in adaptive tree approximation, Numer. Math. 97 (2) (2004) 193–217.
[63] P. Binev, W. Dahmen, R. DeVore, Adaptive finite element methods with convergence rates, Numer. Math. 97 (2) (2004) 219–268.
[64] P. Bringmann, How to prove optimal convergence rates for adaptive least-squares finite element methods, J. Numer. Math. 31 (1) (2023) 43–58, https://doi.org/10.1515/jnma-2021-0116.
[65] P. Bringmann, octAFEM – computational comparison of three adaptive mesh-refinement strategies for the least-squares finite element solution to the Poisson model problem, MATLAB/Octave software package, available on Code Ocean, https://doi.org/10.24433/CO.6310426.v1, 2023.
[66] C. Carstensen, Numerical Analysis Group, AFEM, MATLAB Software Package, 2009, unpublished.
[67] G.H. Golub, J.H. Welsch, Calculation of Gauss quadrature rules, Math. Comput. 23 (1969) 221–230, Addendum, Math. Comput. 23 (106, Loose Microfiche Suppl.) (1969) A1–A10.
[68] W. Gautschi, Orthogonal polynomials in MATLAB, in: Exercises and Solutions, in: Software, Environments, and Tools, vol. 26, Society for Industrial and Applied Mathematics (SIAM), Philadelphia, PA, 2016.
[69] C. Carstensen, F. Hellwig, Constants in discrete Poincaré and Friedrichs inequalities and discrete quasi-interpolation, Comput. Methods Appl. Math. 18 (3) (2018) 433–450.
[70] I.E. Sutherland, G.W. Hodgman, Reentrant polygon clipping, Commun. ACM 17 (1) (1974) 32–42.
[71] H. Rabus, Quasi-optimal convergence of AFEM based on separate marking, Part I, J. Numer. Math. 23 (2) (2015) 137–156.
[72] C. Carstensen, D. Gallistl, F. Hellwig, L. Weggler, Low-order dPG-FEM for an elliptic PDE, Comput. Math. Appl. 68 (11) (2014) 1503–1512.
[73] R.B. Kellogg, On the Poisson equation with intersecting interfaces, Appl. Anal. 4 (1974/1975) 101–129, https://doi.org/10.1080/00036817408839086.
[74] P. Morin, R.H. Nochetto, K.G. Siebert, Data oscillation and convergence of adaptive FEM, SIAM J. Numer. Anal. 38 (2) (2000) 466–488, https://doi.org/10.1137/S0036142999360044.